Federal University of Espírito Santo
Technology Center
Postgraduate Program in Electrical Engineering
Master Thesis

Klaas Minne van der Zwaag

Application of Visible Light Communications in Intensive Care Medical Environments

Vitória, ES, Brazil
August 2020

Klaas Minne van der Zwaag

Application of Visible Light Communications in Intensive Care Medical Environments

This Master thesis was submitted to the Postgraduate Program in Electrical Engineering from the Technology Center of the Federal University of Espírito Santo, as partial requirement for the degree of Master in Electrical Engineering.

Federal University of Espírito Santo – UFES

Electrical Engineering Department

Postgraduation Program

Supervisor: D. Sc. Jair Adriano Lima Silva

Co-supervisor: D. Sc. Teodiano Freire Bastos Filho

Vitória, ES, Brazil

August 2020

Ficha catalográfica disponibilizada pelo Sistema Integrado de Bibliotecas - SIBI/UFES e elaborada pelo autor

---

Zwaag, Klaas Minne Van Der, 1986-

Z97a Application of Visible Light Communications in intensive care medical environments / Klaas Minne Van Der Zwaag. - 2020.

101 f. : il.

Orientador: Jair Adriano Lima Silva.

Coorientador: Teodiano Freire Bastos Filho.

Dissertação (Mestrado em Engenharia Elétrica) - Universidade Federal do Espírito Santo, Centro Tecnológico.

1. Comunicações ópticas. 2. Unidade de tratamento intensivo. 3. Comunicações digitais. 4. Modulação (Eletrônica). 5. Óptica eletrônica. 6. Sistemas de telecomunicação. I. Silva, Jair Adriano Lima. II. Filho, Teodiano Freire Bastos. III. Universidade Federal do Espírito Santo. Centro Tecnológico. IV. Título.

CDU: 621.3

Klaas Minne van der Zwaag

Application of Visible Light Communications in Intensive Care Medical Environments

This Master thesis was submitted to the Postgraduate Program in Electrical Engineering from the Technology Center of the Federal University of Espírito Santo, as partial requirement for the degree of Master in Electrical Engineering.

Work approved. Vitória, ES, Brazil, 28th of August, 2020:

D. Sc. Jair Adriano Lima Silva
Supervisor

D. Sc. Teodiano Freire Bastos Filho
Co-Supervisor

D. Sc. João Crisóstomo Weyl Albuquerque Costa
Universidade Federal do Pará

PhD. Marcelo Eduardo Vieira Segatto
Universidade Federal do Espirito Santo

PhD. Moisés Renato Nunes Ribeiro
Universidade Federal do Espirito Santo

Vitória, ES, Brazil

August 2020

'I Dedicate this Thesis to my Beautiful and Lovely Wife,
Lidiamara Medeiros van der Zwaag,
my Parents Henk and Dettie,
my Brother Jakob
and whole Family van der Zwaag.'

Acknowledgements

I thank God for the knowledge and wisdom, allowing me, despite the circumstances, to conclude this Master Thesis.

Gratefulness to my knowledgeable and dedicated Professor Jair Adriano Lima Silva for his fundamental orientations and Professor Teodiano Freire Bastos Filho for their trust and availability shown to conclude this work.

Special thanks to my precious wife Lidiamara Medeiros van der Zwaag, for the affection, understanding, support and being always at my side.

To Professor Moises Ribeiro and Maria José, for the support and knowledge given since the internship at LabTel as well as Professor Helder Rocha and Marcelo Segatto to conquer this stage of live.

To the company 2Solve, especially Ricardo Calheiros da Conceição and Menno Jan Faber for their dedication, effort and knowledge, making it possible to carry out this work.

To my parents, brothers and sisters of both families Van der Zwaag and Medeiros, for their strength and understanding shown throughout my academic career.

To all my great friends old and new, for always being there for me.

To all Professors and colleagues of LabTel and of the postgraduate Program in Electrical Engineering (PPGEE) at UFES, for the friendship and fellowship.

I also acknowledge the support from the projects TCV-SUS (*Aplicação da Tecnologia de Comunicação por Luz Visível em Monitorização de Recém Nascidos de Alto Risco*) and NEsT-5G (*Núcleo de Estudos em Tecnologias Emergentes para 5G*), which is supported in part by *Fundação de Amparo à Pesquisa e Inovação do Espírito Santo* (FAPES) and in part by *Conselho Nacional de Desenvolvimento Científico e Tecnológico* (CNPq).

'Happy is the man that findeth wisdom,
and the man that getteth understanding.
For the merchandise of it is better than the merchandise of silver,
and the gain thereof than fine gold.
(Holy Bible, Proverbs 3, 13:14)

Abstract

The increasing demand for wireless mobile links with high data rates, high-reliable and low latency requires modern wireless technologies such as 5G and beyond. However, the gradually exhausting radio frequency resources has encouraged scientific investigations on alternative wireless technologies to avoid a future spectrum crunch. Visible light communication (VLC) arose as a promising optical wireless communication technology, exploiting the unlicensed spectrum. Despite the broad free spectrum, VLC offers advantages such as green technology, lack of electromagnetic interference, high security and low power consumption. Existing infrastructure can be utilized employing light emitting diode (LED) for lighting and data transmission simultaneously. In intensive care (IC) medical environments, this technology is an interesting solution to, among others, prevent the spread of emerging diseases. This work present a design, numerical simulations, practical characterizations, as well as experimental performance evaluations of a low-cost, stable and robust VLC system for application in IC medical environments.

Preliminary studies with VLC systems based on orthogonal frequency division multiplexing (OFDM) and constant envelope OFDM signals were addressed considering flicker and light power maximization, respectively. Nevertheless, to accomplish the system complexity requirement, this work focuses on the transmission of on-off keying modulated signals. A proof-of-concept experimental setup is presented and, the results based on the eye opening penalty metric show a comprehensive picture of the proposed VLC system potential. Parameters such as the LED bias current, the modulation frequency, the line-of-sight link distance, the signal pattern and the illuminance sensitivity were extensively evaluated. The results show a susceptibility with correct reception of Manchester coding signals at dimmed illumination levels below 20 and 5 lux, defining the observation/night light standards of IC and ward environments. Error-free performance is demonstrated considering an LED bias current of 400 mA, a signal frequency of 1 MHz and a VLC transmission link length of 2.5 m. Last but not least, captured vital parameters such as heart rate, oxygen saturation, pulse rate, respiration rate, temperature and non-intrusive blood pressure were sent considering an LED polarization current of 400 mA, at VLC links of 1.5, 5 and 15 m. The results obtained with the multi-parametric monitor provide eye-opening-penalty (EOP) values of 0.89, 0.96 and 2.67 dB at the equivalent link distances, proving the feasibility of the proposed VLC system as a promising technology in classified intensive care medical environments.

Keywords: Visible Light Communication, Intensive Care Medical Environments, On-Off Keying, Manchester Codification, Light-Emitting Diode Nonlinearity.

List of Figures

List of Tables

List of abbreviations and acronyms

5G: Fifth-Generation

ADC: Analog-to-Digital converter

AFG: Arbitrary Function Generator

APD: Avalanche Photo-Diode

AWGN: Additive White Gaussian Noise

B2B: Back-to-Back

BER: Bit Error Rate

CE: Constant Envelope

COVID-19: Corona virus

CP: Cyclic Prefix

CSK: Color-Shift Keying

DAC: Digital-to-Analog Converter

dB: Decibel

DC: Direct Current

EA: Electrical Amplifier

ECG: Electrocardiogram

EEG: Electroencephalogram

EMI: Electromagnetic Interference

EO: Eye Opening

EOP: Eye Opening Penalty

E/O: Electrical-to-Optical

EVM: Error Vector Magnitude

FET: Field-Effect transistor

FFT: Fast Fourier Transform

FOV: Field Of View

GaN: Gallium nitride

Ge: Germanium

GHz: Gigahertz

HL7: Health-Life 7 protocol

IC: Intensive Care medical environment

IDFT: Inverse Discrete Fourier Transform

IFFT: Inverse Fast Fourier Transform

IMDD: Intensity-Modulation and Direct-Detection

InGaAs: Indium Gallium Arsenide

IoT: Internet of Things

IR: Infrared

ISI: Intersymbol Interference

LAN: Local Area Network

LED: Light Emitting Diode

Li-Fi: Light-Fidelity

LOS: Line-of-Sight

LUX: Illuminance metric

kHz: Kilohertz

M2M: Machine-to-Machine

MDO: Mixed Domain Oscilloscope

MFTP: Maximum Flickering Time Period

MHz: Megahertz

MIMO: Multiple-Input Multiple-Output

NEP: Noise Equivalent Power

NLOS: Non Line-of-Sight

nm: Nanometer

O/E: Optical-to-Electrical

OFDM: Orthogonal Frequency Division Multiplexing

OOK: On-Off Keying

OWC: Optical Wireless Communication

PAPR: Peak-to-Average Power Ratio

PC: Phosphor Converted LED

PCB: Printed-Circuit Board

PD: Photodiode

PIN: Positive-Intrinsic-Negative

PLC: Power Line Communications

PPM: Pulse Position Modulation

PRBS: Pseudo Random Binary Sequence

PSD: Power Spectral Density

PWM: Pulse Width Modulation

QAM: Quadrature Amplitude Modulation

RF: Radio-Frequency

RGB: Red, Green and Blue

RMS: Root-Mean-Square

RX: Receiver

SI: Silicon

SISO: Single-Input Single-Output

SNR: Signal-to-Noise Ratio

SPO$_2$: Oxygen Saturation

TIA: Trans-Impedance Amplifier

TIC: Technologies Information Communication

THz: Terahertz

TX: Transmitter

UFMC: Universal Filtered Multi-Carrier Modulation

VLC: Visible Light Communications

VPPM: Variable Pulse-Position Modulation

Wi-Fi: Wireless Fidelity

List of symbols

α	Photodiode absorption coefficient
γ	Field-effect transistor noise factor
δ_f	OFDM subcarrier spacing
ε_{ph}	Photon energy
ζ	LED model nonlinearity adjustment constant
η	Photodiode quantum efficiency
η_c	Photodiode fixed capacitance per unit area
θ_n	CE-OFDM phase memory
λ	Wavelength
μ_0	Mean '0' level probability density function
μ_1	Mean '1' level probability density function
π	Pi
$\Pi(t)$	OFDM rectangular pulse-shaping
σ_0	Standard deviation '0' level probability density function
σ_1	Standard deviation '1' level probability density function
σ_{sh}^2	Shot noise variance
σ_{th}^2	Thermal noise variance
ϕ	Channel irradiance angle
$\Phi_{1/2}$	LED semi-angle at half power
$\phi(t)$	CE-OFDM phase signal
ψ	Photodiode incidence angle
Ψ_c	Photodiode field-of-view
∞	Infinity

A	Signal amplitude
A_r	Photodiode surface area
B_{RMS}	CE-OFDM root-mean-square signal bandwidth
B_w	Signal Bandwidth
c	Speed of light
C_N	CE-OFDM variance normalization constant
d	Transmission link distance
d_s	Photodiode semiconductor slab depth
E_b	Energy per bit
EO_{rec}	Received signal eye opening amplitude
EO_{ref}	Reference signal eye opening amplitude
$erfc$	Complementary error function
f	Frequency
f_c	CE-OFDM carrier frequency
$F_{\%}$	Flicker percentage
G	Open-loop voltage gain
g_m	Field-effect transistor transconductance
$g(\psi)$	Channel optical concentrator gain
h	CE-OFDM electrical phase modulation index
h_{LOS}	Channel line-of-sight direct-current gain
h_p	Planck's constant
$h\nu$	Photon energy
I_2	Normalized noise bandwidth factor
I_3	Normalized noise bandwidth factor
I_{DC}	LED bias current
I_{LED}	LED current

I_{SP}	LED modulation current
k	LED model knee factor
K	Boltzmann constant
m	Lambertian emission order
N_0	Noise spectral density
N_{CP}	OFDM cyclic prefix samples
$n_k(nT)$	Zero mean Gaussian noise
N_{sc}	OFDM data subcarriers
P_{DC}	LED bias power
P_{LED}	LED optical output power
P_{max}	LED model maximum output power
P_o	Photodiode incident optical power
P_{rLOS}	Channel received optical power
P_{SP}	LED modulation power
P_t	Channel transmitted optical power
q	Electron charge
Q	Quality-factor
r	Photodiode reflection coefficient (air-semiconductor)
R	OFDM symbol rate
$r_k(nT)$	OOK received signals
R_λ	Photodiode responsivity
$R_o(\phi)$	Channel Lambertian radiant intensity
S_{21}	Transmission gain
$s_k(nT)$	OOK transmitted symbols
$s(t)$	CE-OFDM complex signal
T	CE-OFDM signalling interval duration

T_c	OFDM chip duration
T_k	Thermal noise absolute temperature
T_s	Symbol duration
$T_s(\psi)$	Channel optical filter gain
V_{th}	Threshold voltage
x_k	Pseudorandom binary sequences
$x(t)$	OFDM analog signal
X_k	OFDM complex data symbols
$y(k)$	OOK Demodulated data stream
$y(t)$	CE-OFDM real coefficient signal

Contents

1 Introduction

The necessity of wireless links with high data rates, low latency and reliable connectivity is in its continuous growth process, especially in the use cases predicted in 5G and beyond [7], [8]. Optical wireless communication (OWC) is a wireless communication technology using the unlicensed light spectrum with light sources that provides enough modulation bandwidth for high data rates. Therefore, in the specific light-fidelity (Li-Fi) application, each luminaire, employed as light source, can be used as a wireless access point [9].

The limited availability of radio spectrum has led to an increasing contention between numerous systems, especially in license-free bands. Wireless-fidelity (Wi-Fi) networks are currently experiencing data rate collapses and latency explosions because of the traffic load and, in consequence, interfering traffic. The use of light as a carrier avoids these complications due to the several terahertz available in the unlicensed spectrum, and also due to the fact that interference from other cells is locally confined and can easily be blocked by physical separators or beam adjustment [10], [11].

Visible light communications (VLC) is an optical wireless communication system that transports information through the modulation of a visible light source [12]. According to Rajagopal, Roberts and Lim [13], the visible light spectrum used for communication signals can be determined between 400 THz (780 nm) and 800 THz (380 nm) using light-emitting diodes (LEDs), which are generally applied for illumination. Due to the growth of high power LEDs, interest in VLC has rapidly increased to meet the green technology paradigm. The security in data communication, saving energy, high bandwidth and the possibility of using existing lighting infrastructures are distinct motivations using light to carry information [12].

New technologies are developed to fulfill the demand of the exponential increase of devices requiring wireless connectivity. Due to limitations of radio-frequency (RF) capacity, the unlicensed spectrum used by VLC emerges as a complementary technology to this demand. Through its numerous advantages, VLC technology is subject to research in the areas such as transport, automotive, smart cities, manufacturing, sub-aquatic, and classified areas like health [14, 15, 16]. According to Khan [17], VLC will not interfere or be affected by the radio waves of other machines, and states that the increase of RF to a certain limit results in risks to human health. As there are already many lighting devices installed using LEDs, and the expectation that almost all lighting devices will be LED-based, makes VLC technology a feasible option for optical wireless systems in healthcare environments.

1.1 Motivation

The world is increasingly connected, and the electromagnetic spectrum should have the ability to meet this exponential data growth. The demand of mobile communication is increasing by more than 50% per year, according to the Cisco visual networking index [18]. It is also expected that the number of connected devices will increase from 20 billion to more than 29 billion by 2023, and 70% of the global population will have mobile connectivity [1]. The predictions depicted in Figure 1 indicate that by 2023, half of the 29 billion devices will be mobile connected. Figure 1 also shows that 80% of internet traffic will be video transmission, which requires high transmission speeds (speed average around 20 Mb/s). Furthermore, an increase of 2.4-fold of machine-to-machine (M2M) devices up to 14.7 billion devices, demanding a stable and reliable connection, is expected.

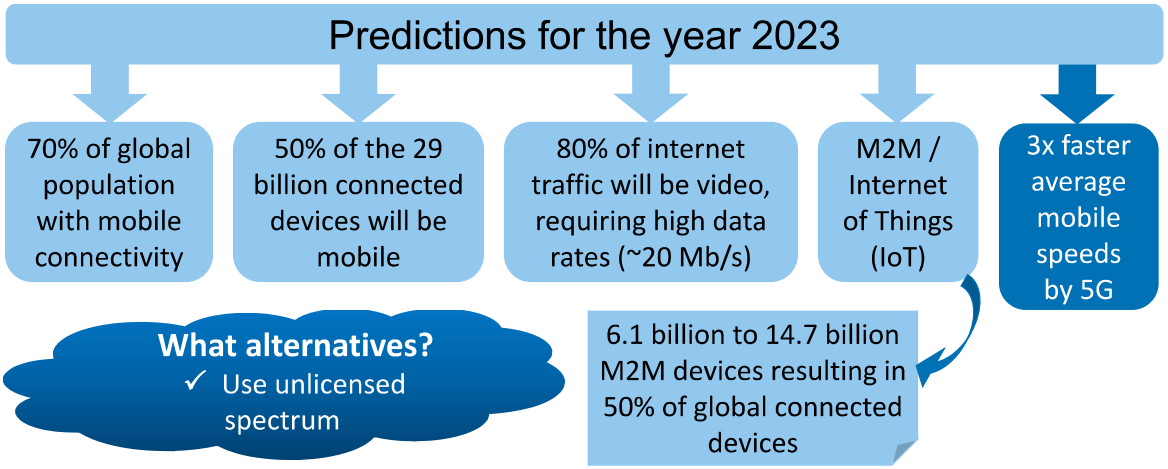

Figure 1 – Mobile communication demand for 2023 [1].

To meet the demand of continuous capacity growth, the use of unlicensed spectrum is required. The implementation of more economical connectivity infrastructures and the increase in number of access points will also be necessary. Therefore, the applications that use the visible light frequencies are promising, since its spectrum is unlicensed and has a bandwidth of 10 thousand times higher than the entire RF bandwidth. Moreover, it should be stressed that the energy consumption and the emission of greenhouse gases can be reduced drastically, by adopting LEDs in general lighting applications and in signaling. The much longer life span and energy savings make the higher costs per LED lamp (when compared with incandescent and fluorescent lamps), economically viable [18].

In classified areas like hospitals, which are sensitive to electromagnetic interference (EMI) or where high security standards are required, VLC finds a wide range of applications because it will not interfere or even be affected by the radio waves of other machines, and

will prevent eavesdropping [17, 19]. On the other hand, monitoring of vital parameters such as temperature, pulse, blood pressure, respiration, electrocardiogram, among others, in hospital intensive care (IC) units is extremely important for rapid and effective interventions, aimed the patients returning to baseline conditions. Thus, VLC can provide access of vital parameters to a doctor and/or nurse on personal devices such as smartphones and/or a tablets [20].

To provide a better diagnosis and better patient experience, eHealth has been proposed as a complement to traditional health services. According to the world health organization, eHealth is the use of technologies, information and communication (TIC) in health [21]. In recent years the number of health solutions with medical devices and information systems connected through wired or wireless networks has grown. Systems that exploit VLC technology have been widely suggested and experienced in many areas of knowledge, because of their superior benefits compared to other wireless transmission alternatives such as Wi-Fi [22]. The advantages of wireless communication systems are contrasted with communication restrictions in classified areas as those that characterize IC and surgery environments.

Another important aspect is prevention and spreading of diseases, especially at this moment of writing the worldwide situation concerning COVID-19. Most of the medical devices are connected by a cable for power and network connection in a local area network (LAN). Practice shows that transportation of equipment with cables between two distinct locations can contribute the spread of bacteria and/or viruses [23].

In this context, communication via visible light arises as a wireless technology of wide bandwidth data transmission, which uses LEDs as devices to transmit vital parameters of the patient's health. Therefore, beyond the prevention of diseases spreading, VLC presents itself as a safer, efficient and innovative solution, since most health systems require a signal free of electromagnetic interference and a secure communication [21].

1.2 Literature Review

Several studies on VLC in distinct applications have been published [24], although research related to the transmission of patients information by VLC in hospitals is sparse. Perceived by human eyes, the flicker phenomenon, that induces physiological changes in human beings, became one of the first subjects studied in this area [13, 25, 26, 27, 28]. Accepting that the intensity of flicker depends on both frequency and amplitude of optical modulated waveforms, the use of a frequency greater than 200 Hz was stated as a safe value in VLC deployments [28], [13]. Nevertheless, the preoccupation with high amplitude fluctuations of the optical signals remain, especially in the case when a human is being exposed in an

ambient for a long time [29].

VLC is often investigated for wearable patient monitoring devices. In some cases, a VLC downlink with an infrared (IR) uplink is proposed like in [30], or entirely with an IR mobility scheme as described in [31]. The downside of these schemes is the possible interference with some medical equipment like surgeon robots, where IR optical tracking systems are used [32]. The respective authors also performed experiments with VLC in a hospital surgery room, using different Li-Fi schemes with a multi-user multiple-input multiple-output (MIMO) link to create a robust transmission. To avoid the aforementioned IR and electromagnetic interference, the authors of [33] deployed VLC to avoid EMI on patient monitoring systems. In their work, they achieved a 30 cm optical link to transmit electrocardiogram (ECG) signals using on-off-keying (OOK) modulation. EMI is proven in a clinical laboratory on equipment by Badizadegan in [34], where the interference caused erroneous clinical results.

On-off keying modulation technology is used in various simulations and experimental setups to achieve a reliable and stable connection. According to the experimental work provided in [35], an uncollimated line-of-sight (LOS) transmission link over 50 cm, with ECG data at a rate of 56 kbps, is achievable with the OOK format. In order to create a reliable ECG transmission, the authors of [36] created a scheme based on OOK and a 81-LED array. In [37] and [38] the authors, based on simulations, state that, for a multiple-patient optical body area network with all vital parameters, a highly reliable transmission can be achieved using OOK with RGB and white LEDs. In [39], Kumari and Samiappan successfully show a VLC system that transmit all vital data over a distance of 20 cm, also using OOK modulation in their experimental prototype. However, the relatively short reach achieved in the above-mentioned works is an issue to be addressed.

In [40], posturometry data is transmitted with a prototype over a distance of 2 m with an OOK modulated signal at 66 Hz, whereas in [41] the authors created an OOK based VLC uplink prototype for patient information, resulting in an VLC LOS link over 1.3 m at a speed of 10 bps. In these cases, the extremely low transmission rates can be treated as prohibitive in videos and/or image applications.

Other modulation schemes such as pulse position and pulse width modulations (PPM and PWM), as well as orthogonal frequency division multiplexing (OFDM) were also suggested for VLC application in hospitals. Huang and Zhang show, in [42], conducted simulations of a VLC positioning system based on dark light technology, where a short high intensity pulse with a minimum frequency of 160 Hz is codified through PPM. They state that the high intense short pulse will not be perceived by the human eye and is suitable for dimming schemes. Aiming to combat a reduction of reliability, efficiency and accuracy through RF signals, Ilakkiaselvan et al. applied an experimental VLC research

sending ECG signals using PWM modulation [43]. To create an integrated system where the existing infrastructure can be utilized, a hybrid system with a combination of VLC and power line communications (PLC) for hospitals is proposed in [44]. By increasing the systems complexity, the authors employed pre-equalization to achieve a transmission link of 5 m, with a 48 Mbps OFDM technique. As can be seen, most of the research is carried out with ECG signals, and monitoring of multi-parametric monitor parameters was not considered. Due to its implementation simplicity and, in consequence, to the cost benefit, OOK is the requested format for applications such as the one attended in this work.

Nowadays, navigation improvements using VLC in hospitals seems to be a research hot topic. This was carried out with hospital delivery robots by using VLC in addition to existing technologies. In [45], Murai and contributors carried this solution in practice where every luminaire has its own identification sequence to help the robots to obtain more information about the environment.

1.3 Objectives of this Work

The general objective of this work was to propose and evaluate the robustness of a low cost, stable and reliable VLC transmission system for application in intensive care medical environments. Numerical simulations and proof-of-concept experimental demonstrations were conducted to evaluate the performance of the modulation and detection schemes. To accomplish the main objective, the following specific objectives have to be achieved:

- (i) Comprehensive study and numerical simulations of VLC channel models with the purpose of system parameters design;
- (ii) Extensive simulations on the modulation techniques, aiming a stable, robust and flicker free VLC connection;
- (iii) Performance evaluations of the modulation techniques, regarding an analysis of the systems physical and optical limitations;
- (iv) Development and assembly of an experimental setup to be used in the envisioned proof-of-concepts;
- (v) Experimental demonstrations of modulated signal transmissions over line-of-sight (LOS) VLC systems;
- (vi) Validation of the aforementioned proof with data generated by a multi-parametric monitor normally used in IC medical environments.

1.4 Methodology

The first stages of this research included a bibliographic review on the developed subject. The exploratory nature of the research, demonstrated by the bibliographic review, provided a deep understand of VLC communication systems and its impact on the current market. An extensive study on the modulation formats used in VLC, as well as the models of existing optical channels, was accomplished prior the numerical simulations. A set of simulations was then executed considering the transmission of OFDM, constant-envelope OFDM (CE-OFDM) and OOK with Manchester codification, aiming adjustments of the numerical models through parameters design. Numerical simulations were performed to evaluate the robustness of these models in VLC systems with LOS channels.

The next step consisted on the characterization of all parts of the experimental setup individually, consisting, among others, of a self-designed VLC transmitter and receiver prototypes, properly tested, in order to find the factors that could limit the performance of the VLC system. The assembly of an experimental setup and validation tests with Manchester line code follows the numerical studies in order to proof the concepts employed in the research. The experimental results obtained in terms of the metrics bit-error-rate (BER) and eye opening penalty (EOP), and their analysis considering different distances, frequencies and LED drive currents, highlighted the quantitative nature of the research.

To emulate an hospital IC environment, data from the PRO12 multi-parametric monitor is sent through the prepared VLC transmitter and captured by the receiver prototype built for this purpose. It should be noticed that, the research and the technological development described in this Master Thesis is part of the subjects to be addressed in the projects **TCV-SUS** (*Aplicação da **T**ecnologia de **C**omunicação por Luz **V**isível em Monitorização de Recém Nascidos de Alto Risco*) and **NEsT-5G** (***N**úcleo de **Es**tudos em **T**ecnologias Emergentes para **5G***) supported in part by *Fundação de Amparo à Pesquisa e Inovação do Espírito Santo* (FAPES) and in part by *Conselho Nacional de Desenvolvimento Científico e Tecnológico* (CNPq).

The scenario depicted in Figure 2 represents one of the applications proposed in the above-mentioned projects, in which VLC serves as a backup communication technology in hospital IC environments. As an alternative to the LAN, this technology should be able to transfer the multi-parametric parameters to personal devices of the medical team. The emulation described in this work only took into account the visible light communication part.

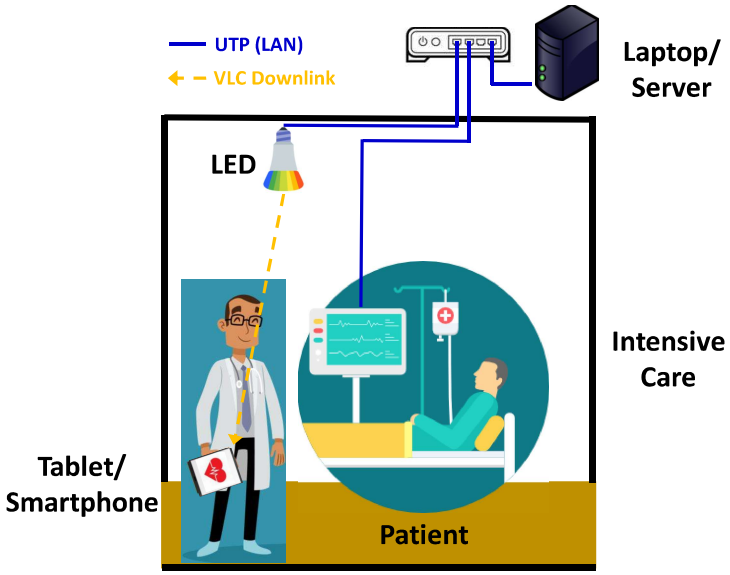

Figure 2 – Intensive care environment also envisioned for proof-of-concepts.

1.5 Main Contributions of this Work

Beyond the present document, three principal contributions of the research must be highlighted. The numerical model developed to evaluate the performance of Manchester coding signals through LOS VLC systems represents the first contribution, that certainly will assist the studies designated in the **TCV-SUS** and **NEsT-5G** projects. The model was tested through the large quantity of accomplished simulations, where the parameters such as distance, LED polarization current and frequency were adjusted aiming the optimum performance of the VLC system.

The construction of a self-made low cost and straightforward VLC transmitter, as well as a visible light photodetection receiver that allowed, through experimental assembly, the validation of the implemented numerical model is another important contribution of this work. The constructed and properly tested transceiver is now available in LabTel for future VLC projects, and further replications can be easily produced for the practical implementation of the scenario shown in Figure 2, in **HUCAM** (*Hospital Universitário Cassiano Antonio Moraes*) and in others hospitals of **SUS** (*Sistema Único de Saúde*).

Finally, the emphasis reserved to the transmission of the PRO12 multi-parametric monitor data through the evaluated VLC system represented a special contribution of the research at all. Part of the results obtained at the end of this work allowed the publication and/or submission of the following scientific articles:

- **Klaas M. vd Zwaag**, José L. C. Neves, Helder R. O. Rocha, Marcelo E. V. Segatto, e Jair A. L. Silva. **Increasing VLC Non-linearity Tolerance by CE-OFDM**, OSA Latin America & Photonics Conference (LAOP) 2018, Lima, Peru.

<https://doi.org/10.1364/LAOP.2018.W3D.3>;

- **Klaas M. vd Zwaag**, José L. C., Neves, Helder R. O. Rocha, Marcelo E. V. Segatto, e Jair A. L. Silva. **Adaptation to the LEDs flicker requirement in visible light communication systems through CE-OFDM signals**, Optics Communications, vol. 441, pp. 14–20, 2019, Elsevier. <https://doi.org/10.1016/j.optcom.2019.02.017>;
- **Klaas M. vd Zwaag**, Lidiamara M. vd Zwaag, Jair A. L. Silva, Helder R. O. Rocha, Marcelo E. V. Segatto, e Teodiano F. B. Filho. **Impact of the Signal Bandwidth in an OOK-based VLC System: Evaluation in Intensive Care Applications**, Presented at *Optical Wireless Communication Conference* (Eindhoven, Netherlands, 2020);
- **Klaas vd Zwaag** et. al., **A Manchester-OOK Visible Light Communication System for Patient Monitoring in Intensive Care Units**, submitted to *IEEE Access*.
- **Klaas vd Zwaag** et. al., **Performance Evaluation of an OOK-based Visible Light Communication System for Transmission of Patient Monitoring**, IFMBE Proceedings, vol. 83, 2021, Springer. <https://doi.org/10.1007/978-3-030-70601-2>, and presented at *Congresso Brasileiro de Engenharia Biomédica* (CBEB 2020);
- R. Lazaro, **Klaas vd Zwaag** et. al., **Integrating Power Line and Visible Light Communication Technologies for Data Transmission in Hospital Environments**, IFMBE Proceedings, vol. 83, 2021, Springer. <https://doi.org/10.1007/978-3-030-70601-2>, and presented at *Congresso Brasileiro de Engenharia Biomédica* (CBEB 2020);
- A. Santos, **Klaas vd Zwaag** et. al., **Aplicação da Tecnologia de Comunicação via Luz Visível para Monitorização em Hospitais**, Presented at *Congresso Brasileiro de Engenharia Biomédica* (CBEB 2020);
- José Neves, **Klaas vd Zwaag**, Wesley Costa, Helder Rocha, Marcelo Segatto, Jair Silva, Malte Hinrichs, Anagnostis Paraskevopoulos, Volker Jungnickel, Ronald Freund. **CE-OFDM in Visible Light Communications**, to be submitted in *IEEE Photonics Technology Letters*;

1.6 Organization of this Work

The remainder of this work is organized as follows. Chapter 2 presents an in-depth study of the basic elements of a LOS VLC system, with a particular emphasis in the nonlinearity provided by LEDs. Important discussions related to OFDM, CE-OFDM

and OOK modulation formats in VLC systems, as well as about the simulation results that described the stability, robustness and the flicker phenomenon, are carried out in Chapter 3. Chapter 4 is intended for the presentation of the experimental setup and the electrical and optical characterization of each single used component, to accomplish the proper functioning of the proof-of-concept. Experimental validation by an extensive performance analysis with Manchester modulated signals, transmitted over LOS VLC channels, are shown in Chapter 5. The descriptions provided in Chapter 5 also demonstrate the satisfying experimental proof of a simulated intensive care medical environment, with a multi-parametric patient monitor sending and recovering successfully obtained sensor data over various distances. Conclusions and future works are provided in Chapter 6.

2 Visible Light Communication

In 1880, Alexander Graham Bell achieved a historical landmark with visible light in an unguided channel [46]. Bell modulated the solar radiation with the voice signal using a diaphragm mounted on a mirror transmitting to distances of about 200 m. In his experiment, he showed, for the first time, the basic principle of modern optical communications [47, 48]. Because of the rudimentary form, the intermittent nature of solar radiation and changing weather conditions, the photophone was not commercially successful. After a period of relative small achievements, communication based on visible light experienced a revival [49]. Improvement in efficacy and lower costs of light generation and limited availability of radio spectrum, caused by the increased data use and smart devices, contributed to this new impulse of OWC systems [50]. Due to this, the demand for high speed connections is expended and research to unlicensed spectrum technologies intensified.

In the current state of VLC research, the main projects are focused on Li-Fi networks, which is an optical wireless network using VLC technology to provide bidirectional multi-user communication, mobility and high transmission rates [48]. In 2017, to highlight some important results, researchers achieved a data rate of 17.6 Gb/s in a 16 m VLC link using a blue LED, 16-QAM based universal filtered multi-carrier (UFMC) modulation and an ultra-fast photodetector [51]. In [52], the authors presented a white-light communication link based on laser diodes with a microelectromechanical system mirror-based beam-steering, where the researchers achieved a data rate of 35 Gb/s at a link distance of 4 m and 39 m^2 of coverage. In 2020, 7.7 Gbps of data transmission rate was achieved with the authors of [53]. A single 10 μm gallium nitride (GaN) blue microLED transmitting data over a 18.5 cm distance was successfully demonstrated in their experiments.

VLC is the result of the recently achieved development in LED lighting technology. The widespread use of LEDs in various applications represents an opportunity for VLC. Large bandwidth, security in data communication, no electromagnetic interference, lighting and/or energy saving are the main features that have made VLC an emerging technology for short-range internal communications and a compelling field of worldwide research [54].

2.1 VLC System Model

VLC is a system that combines illumination of lasers or LEDs with light modulation for data communication [12]. By modulating light intensity in the visible light spectrum range (380 - 780 nm), through switching on and off the light source at high speed, VLC systems transmit data not perceived by the human eye [46, 12, 49]. The contrast of RF and VLC

bandwidth is depicted in Figure 3, showing that the bandwidth of the unlicensed spectrum is up to ≈ 10.000x larger, and thus one of the potentials of VLC [55].

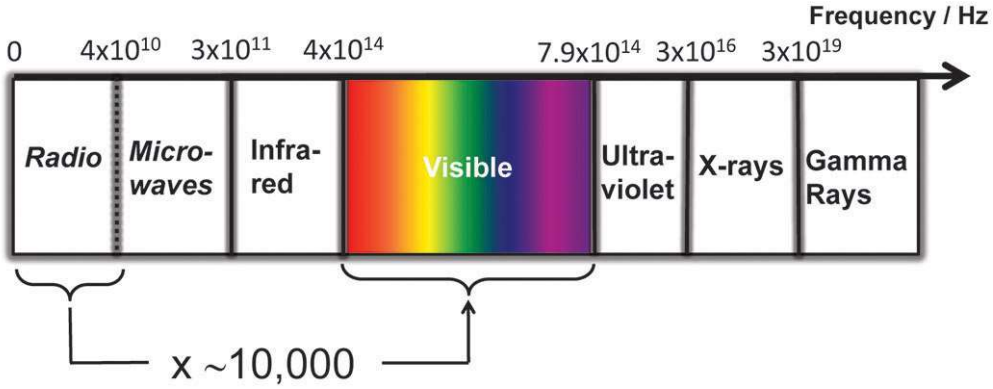

Figure 3 – The electromagnetic spectrum comparing the RF and VLC bandwidth [2].

LEDs are the preferred choice over lasers when both lighting and data transmission are requested in certain applications. Nevertheless, as medium for data communication and illumination in environments like hospitals, LEDs has to propagate white light [49, 56]. In Figure 4, the VLC system fundamentals are shown, consisting of a transmitter, a wireless channel and a receiver. The transmitter includes a part of data encoding, an LED and its driver used to adapt the encoded signals for transmission in an intensity-modulation and direct-detection (IMDD) optical system.

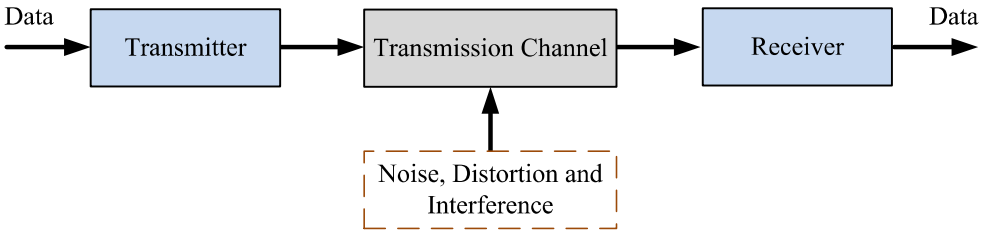

Figure 4 – Basic elements of a VLC system

The optical beams with data signals propagate through the wireless channel, during which they suffer progressive attenuation and diverse types of interference/noise, such as sunlight, coupling incandescent and fluorescent light, among others. Therefore, amplitude distortions provided by channel gain variations in the used bandwidth, and phase distortions determined by different time delays suffered by the spectral components at different frequencies should be considered in signal recovering. The receiver includes an opto-electric conversion device like a photodiode, a signal post-processing and a decoding scheme to treat the received signals. The signals are filtered and amplified to compensate the transmission loss, before equalization processing that can be applied to compensate amplitude and phase distortions. The signal is then demodulated and decoded to recover the original signal [57].

2.2 Transceiver Front-Ends

The front-end of a VLC transmitter consists of an electrical-to-optical (E/O) converter used as optical source, along with auxiliary elements employed to activate the light source. Due to its efficacy and low-cost implementation, high brightness white LEDs are commonly applied for illumination and communication. From the perspective of communication, LEDs are desirable above conventional lamps, since LEDs have a much faster response, varying the intensity of emitting photons [58], which is also faster than the persistence of the human eye [13, 59]. In its turn, the front-end of a VLC receiver consists of an optical-to-electrical (O/E) conversion, in which the received optical power produces a proportional electrical current. Since no phase, frequency or polarization sensitivity is required to detect the intensity of the optical field, positive-intrinsic-negative (PIN) or avalanche photo-diodes (APD) photodiodes are commonly used in the detection of the optical field [60].

2.2.1 Light-Emitting Diodes

A light-emitting diode is an optoelectronic device made of semiconductor materials that transforms electrical energy into light. The emergence of high brightness LEDs revolutionized conventional lighting methods and paved the way for visible light to become a realistic medium for data communications [61]. In 1999, Pang proposed the first application with an LED as a data communication device in the visible range [62]. However, interest in this type of communication gained more attention in 2003, with the work described in [63], where an LED was used simultaneously as a lighting and communication device.

The basic structure of an LED is composed of a P-N semiconductor junction, subject to direct polarization voltage. This type of light generation is more efficient then conventional lighting due to lower energy consumption. Therefore, LEDs have a positive impact on the greenhouse effect by reducing CO_2, making it an environment friendly technology for the future [64]. When a direct voltage is applied through the P-N junction, electrons and gaps are injected through the depletion region, causing excess minority carriers to recombine with the majority carriers, giving rise to energy release under the form of light (observation electroluminescence). This spontaneous radiating released energy is the basis of operation of the LEDs. The wavelength of the light emitted by the LED is inversely proportional to the energy of the prohibited band. The greater the energy of the emitted photon, the shorter the wavelength. Equation (2.1) relates the wavelength to the photon energy as

$$\lambda = \frac{h_p \times c}{\varepsilon_{ph}}, \tag{2.1}$$

where λ is the wavelength expressed in micrometers, h_p is Planck's constant ($h_p =$

6.63×10^{-34} Js $= 4.14 \times 10^{-15}$ eV), c is the speed of light ($c = 3 \times 10^{8}$ ms^{-1}) and ε_{ph} is the photon energy expressed in electron volt (1 eV $= 1,602 \times 10^{-19}$ J). It can be seen from Equation (2.1) that the LED material influences the operation wavelength.

Normally, in VLC applications there are essentially two types of white light generation. One with a single blue LED die with a yellow phosphor layer (PC-LED) and the second composed of a multi-die LED with red, green and blue (RGB) light as shown in Figure 5. Due to the lower costs, complexity and good color rendering index, the vast majority of high-brightness white LEDs on the market use currently the phosphor conversion principle to generate white light. However, from the perspective of VLC, the PC-LED is limited by the restricted 3 dB bandwidth of $2 - 3$ MHz of the yellow phosphor caused by the slow absorbing and re-emission capacity of the photons [65].

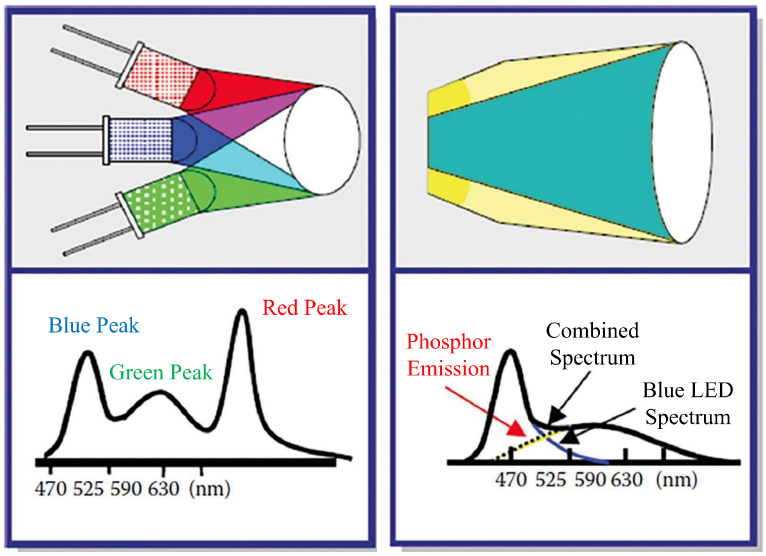

Figure 5 – White light generation based on: (a) red, green and blue LEDs; (b) blue LED and yellow phosphor [3].

Due to higher costs and complexity, RGB LEDs are more applied in dynamic lighting than in general lighting systems. Despite these disadvantages, RGB LEDs are preferred in high speed VLC systems due to the superior modulation bandwidth ranging from 10 to 20 MHz [66, 67]. Table 1 shows a comparison between RGB and PC-LED based technologies.

2.2.2 Positive-Intrinsic-Negative Photodiodes

A photodiode is a semiconductor device that converts light into electrical energy in the presence of light. High sensitivity for the wavelengths of interest, high bandwidth and response times adequate to the used data rates, minimum noise, low sensitivity to variations in environmental conditions and long average lifetimes are some desirable characteristics in photodetectors [68]. An APD has a much higher gain than the PIN photodiode, however,

Table 1 – Comparison between RGB and phosphor converted LED technologies [4, 5].

Parameter	**Phosphor coated LED**	**RGB LED**
Bandwidth	2-5 MHz	10-20 MHz
Luminous efficiency	150 lm/W	65 lm/W
Cost	low	high
Complexity	low	moderate
Application	Illumination	Illumination

the excess noise generated by its photocurrent is considered a disadvantage compared to PIN photodiodes [4]. The PIN photodetector is used very often in VLC systems because of its high temperature tolerance, lower cost and is suitable in bright environments. Therefore, the focus of this work is on PIN photodetectors.

A PIN photodiode is composed of a P-N junction with a layer of intrinsic semiconductor material placed between the P-type and the N-type materials. The intrinsic layer is optically active and acts as a depletion region for the device. In addition, it is placed in order to increase the optical exposure and also to reduce the intrinsic capacitance of the photodetector. The PIN photodiode operates with reverse polarization, which means that incident photons are absorbed in the depletion region, where there is an intense electric field. The presence of the electric field ensures that the photo-generated carriers are quickly separated and collected in the P (gaps) and N (electrons) regions of the photodetector, before its recombination [69]. The electrical current I at the output of a photodiode is given by

$$I = P_o \frac{q\lambda}{h_p c}(1-r)\left(1 - e^{\alpha(\lambda)d_s}\right), \tag{2.2}$$

where P_o is the incident optical power, r is the reflection coefficient at the air-semiconductor interface, α is the absorption coefficient, d_s is the depth of the semiconductor slab, q is the electron charge, c is the speed of light and h_p is Planck's constant.

Responsiveness, $R_\lambda = \frac{I}{P_o}$ in A/W, is another parameter that characterizes photodiodes, relating the electrical current at the output of the photodiode to the incident optical power. Knowing that the quantum efficiency is mathematically expressed as $\eta = \frac{I/q}{P_o/(h_p\nu)}$, Equation 2.3 provides the mathematical expression that relates quantum efficiency with responsivity [70], [69] as

$$R_\lambda = \frac{\eta q}{h_p \nu} = \eta \frac{q\lambda}{h_p c} = \eta \frac{\lambda[\mu m]}{1.24}. \tag{2.3}$$

It is important to notice that silicon (Si), and indium gallium arsenide (InGaAs) exhibit responsivity close to the theoretical limit imposed by a quantum efficiency of 90 %, which means that in the detection of visible light radiation, Si and GaAs are the most

favorable semiconductors. The transit time of carriers photo-generated through the region of depletion, the frequency response limited by the RC time constant, which depends on the capacitance of the diode, and the slow diffusion of carriers generated outside the depletion region are factors that have a considerable impact on the bandwidth and response speed of a photodetector. [6]. Typical values of PIN parameters for Si, germanium (Ge), and InGaAs are listed in Table 2.

Table 2 – PIN performance characteristics comparison [6].

	PIN Photodiode		
Parameter	**Si**	**Ge**	**InGaAs**
Wavelength λ (nm)	400 – 1100	800 – 1800	900 - 1700
Peak λ (nm)	900	1550	1300 (1500)
R_λ (A/W)	0.6	0.65 – 0.7	0.63 – 0.8 (0.75 – 0.97)
η (%)	65 – 90	50 – 55	60 – 70
Gain (M)	1	1	1
Polarization Voltage (V)	45 – 100	6 – 10	5
Dark current (nA)	1 – 10	50 – 500	1 – 20
Capacitance (pF)	1.2 – 3	2 – 5	0.5 – 2
Rise Time (ns)	0.5 – 1	0.1 – 0.5	0.06 – 0.5

The dark current is the current that appears at the output of the photodiode in the absence of light. It includes the photocurrent generated by the background radiation and the saturation current of the semiconductor junction. The dark current establishes a minimum threshold in the current detectable by the photodiode, that is, a signal to be detected must produce a current greater than it. The dark current depends on the operating temperature, the bias voltage and the type of detector. Often, depending on the application, it is interpreted as a source of noise [6]. The equivalent power of the noise equivalent power (NEP) is the minimum optical input power capable of generating photocurrent. It is equal to the effective value of the noise current in a bandwidth of 1 Hz. The NEP depends on the frequency of the modulated signal, the bandwidth in which the noise is measured, the area of the photodetector and the operating temperature.

2.2.3 Trans-Impedance Amplification

It should be stressed that, in order to support the establishment of an LOS communication scenario, the first part of the signal reception should employ an optical lens or an optical concentrator to concentrate the light on the detection surface of the photodiode, and therefore improve the signal-to-noise ratio. An optical filter can also be used to reduce the effect of optical noise produced by the environment [71].

Nevertheless, a pre-amplifier is mandatory after the photodetection to amplify the signal before its processing. The amplifiers used in VLC can be classified into three categories: low impedance, high impedance and trans-impedance amplifier (TIA). The choice of the type of amplifier depends on a compromise between speed and sensitivity. The high impedance amplifier improves sensitivity by reducing thermal noise, but has low bandwidth. With the low impedance amplifier, thermal noise prevails, making this type of amplifier impractical in VLC systems. The TIA amplifier is most popular in the VLC system, as it guarantees high sensitivity and high bandwidth [4]. The other parts of the VLC receiver consists of a signal processing stage and a demodulation stage, similar to conventional receivers.

2.3 VLC Channel Modeling

Similar to infrared links, indoor VLC can be classified in LOS links and in diffuse non-line-of-sight (NLOS) links [72]. With carefully aligned transceivers, a LOS communication can support high transmission speeds by focusing the transmission beam and using a narrow receiver field-of-view (FOV). In a non-directed link, the communication between a divergent transmitted beam and a large FOV receiver strongly depends on surface signal reflections [49]. Even operating in the absence of LOS, a non-directed link can be robust to shadowing and can inherently support user mobility, despite the power and data rate limitations provided by multi-path propagation effects [72, 73]. As mentioned above, the application exploited in this work considers a LOS link in a single-input single-output (SISO) communication scenario.

2.3.1 An LOS Channel Model

In an LOS link, the received optical power is generally determined as $P_{rLOS} = h_{LOS} \times P_t$, for P_t the average transmitted optical power and h_{LOS} the channel DC gain given by

$$h_{LOS} = \begin{cases} \frac{A_r}{d^2} R_o(\phi) T_s(\psi) g(\psi) \cos(\psi), & 0 \leq \psi \leq \Psi_c \\ 0, & \psi > \Psi_c, \end{cases} \tag{2.4}$$

where A_r denotes the photodetector area, d is the distance between transmitter and receiver, ϕ is the irradiance angle, ψ is the angle of incidence, $T_s(\psi)$ is the gain of an optical filter, $g(\psi)$ is the gain of an optical concentrator that depends on the refractive index, and Ψ_c is the receiver FOV [49, 72, 74]. In Equation 2.4, $R_o(\phi)$ represents the Lambertian radiant intensity given by

$$R_o(\phi) = \frac{m+1}{2\pi} (\cos(\phi))^m, \tag{2.5}$$

for m the order of Lambertian emission, which is related to the LED semi-angle at half power denoted as $\Phi_{1/2}$, and is mathematically defined as

$$m = -\frac{\ln(2)}{\ln(\cos(\Phi_{1/2}))}. \tag{2.6}$$

2.3.2 Typical Sources of Noise

Even known that the multipath components of the NLOS are neglected in the link structure studied in this work, the received signal $r(t)$ is defined as $r(t) = s(t) \times h_{LOS} + n(t)$, for $s(t)$ the optical modulated signal and $n(t)$ the received noise at the photodiode, that can be modeled as an additive white Gaussian noise (AWGN) with zero mean and variance given by

$$\sigma^2 = \sigma_{sh}^2 + \sigma_{th}^2, \tag{2.7}$$

where σ_{sh}^2 is the variances of the shot noise and σ_{th}^2 the variance of the thermal noise [75]. In the scenario considered in this work, the shot noise can be neglected due to the transmission with low data rates, unlike the thermal noise that results from the transimpedance receiver circuitry, and has a variance given by

$$\sigma_{th}^2 = \frac{8\pi K T_k}{G}\eta_c A_r I_2 B_w^2 + \frac{16\pi^2 K T_k \gamma}{g_m}\eta_c A_r^2 I_3 B^3, \tag{2.8}$$

in which, K denotes the Boltzmann's constant, T_k the absolute temperature, G the open-loop voltage gain, η_c the photodiode fixed capacitance per unit area A_r, I_2 a noise bandwidth factor, B_w the signal bandwidth, γ the field-effect transistor noise factor, g_m the FET transconductance, and the normalized noise bandwidth factor $I_3 = 0.0868$ [74].

2.4 Analysis of the LED Nonlinearity

In the optical intensity modulation that supports VLC, the modulated data varies the luminous intensity of an LED. That is, the output optical power of a source varies according to the characteristics of the modulated signal [60]. Therefore, the LED should be biased before applying the modulating signal since the optical intensity cannot be negative. In the case of current-based driving circuit, this means that the electrical modulated signal I_{SP} (which is proportional to $s(t)$) is superimposed onto the LED bias current I_{DC}, providing an LED current $I_{LED} = I_{DC} + I_{SP}$. The current I_{LED} produces an optical output power given by

$$P_{LED} = P_{DC} + P_{SP}, \tag{2.9}$$

for P_{DC} and P_{SP} the powers of the bias current and the swinging current component, respectively. Figure 6 shows a theoretical behavior of the optical power output as a function

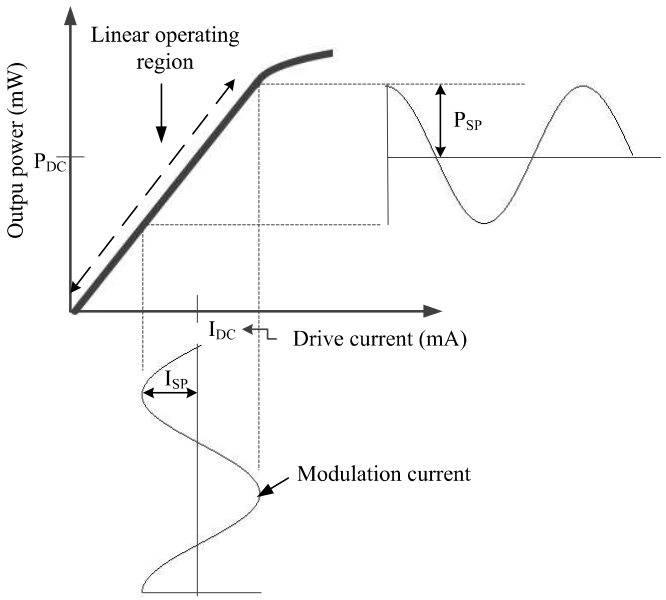

Figure 6 – The theoretical current-power curve of an LED.

of the current flowing through the LED. It can be seen from Figure 6 that there is a maximum amplitude swing limitation that also limits the optical output power.

The direct current is usually concentrated in the linear region of the characteristic curve depicted in Figure 6, since the LED's response exhibits nonlinearity for large input signals. Increasing the magnitude of the modulating signal will drive the LED into the nonlinear region, thus distorting the output optical signal. Therefore, in the design of the modulation scheme in LED-based VLC systems, a trade-off between optical power maximization and LED introduced nonlinearity should be investigated.

The curve illustrated in Figure 6 can also express the behaviour of a voltage-current characteristic, however, with a current versus optical power particularity. If the last case is of interest, the nonlinearity of the LED can be theoretically expressed as follows

$$P_{LED} = \frac{I_{LED}}{\left[\zeta + \left(\frac{I_{LED}}{P_{max}}\right)^{2k}\right]^{1/2k}}, \tag{2.10}$$

for P_{max} the maximum output power, ζ an adjustment constant and k a knee factor also used to fit the characteristic curve [76]. Figure 7(b) shows a plot of this model, as well as the result of a measurement of optical intensity in lux against LED bias current. To fit the model with the measurement, the following parameter values were used: $P_{max} = 755$ lux, $\zeta = 20$ and $k = 1.9$. A photo of the experimental setup used to measure the characteristic is shown in Figure 7(a). The agreement between the theoretical and the experimental measurement indicates that the model presented at Equation (2.10) allows emulating the nonlinearity behaviour of the white LED.

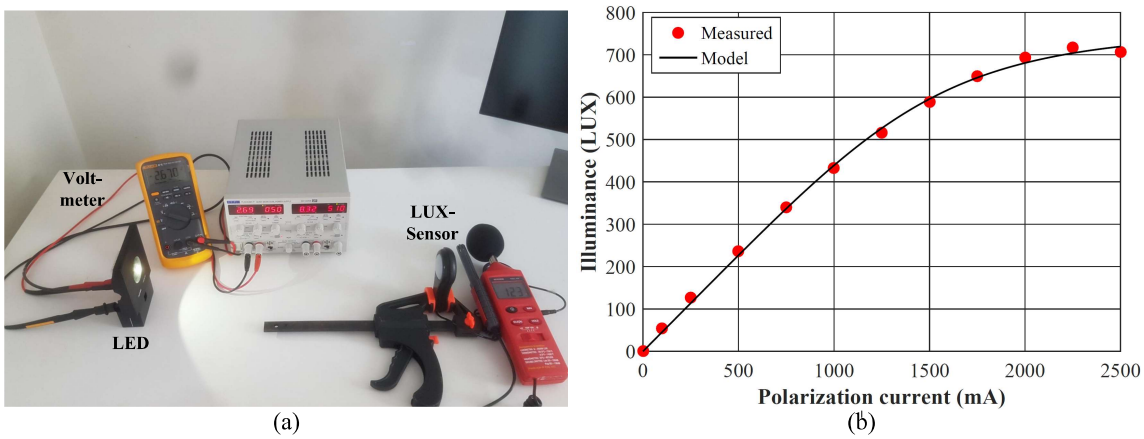

(a) (b)

Figure 7 – Experimental current-lux curve measurement: (a) the used setup; (b) the analytical and the experimental curves of the LED.

3 Modulation Schemes

During a VLC, the LED average optical power may change, giving rise to the flicker phenomenon, normally defined as the fluctuation of the brightness caused by modulating the light intensity. Perceived by human eyes, this inconvenience induces physiological changes in human beings, which is potentialized by high levels of illuminance, long duration of exposure in the communication ambient and orientation of the light source with respect to the eyes [13, 25, 26, 27, 28]. Hence, it is acceptable that the intensity of flicker depends on both frequency and amplitude of optical modulated waveforms [28]. An investigation on the modulation schemes, that takes into account this phenomena, as well as the maximization of optical power, aiming reach extension, is essential.

3.1 The Flicker Concept

Generally quantified by metrics such as flicker index and percent flicker (equivalent to modulation depth), the flicker is mathematically related to the modulated signal amplitudes, despite the above-mentioned frequency association [26]. It can be seen from Figure 8 that the percent flicker ($F_{\%}$) takes into account the maximum (A) and minimum (B) amplitudes of the modulated waveforms.

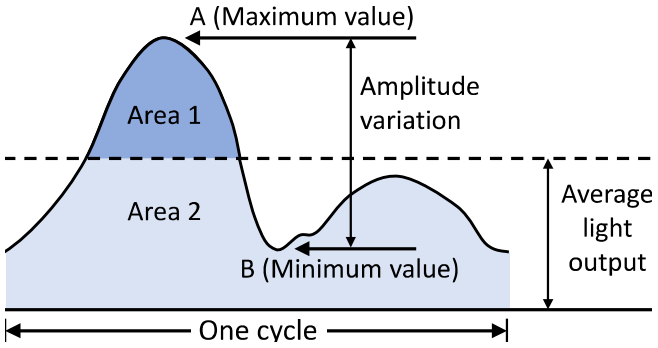

Figure 8 – Illustrative definition of percent flicker and flicker index.

Hence, for sake of simplicity, ($F_{\%}$) is used to quantify flicker, mathematically expressed as

$$F_{\%} = 100\% \times \frac{A - B}{A + B}, \tag{3.1}$$

in which it is easy to conclude that, when the percent flicker decreases, flicker becomes less noticeable to the human eye. It should be stressed that commercial off the shelf LEDs has common values of $F_{\%}$ around 1 %, 16.96 %, 19.63 %, 21.27 %, 29.41 %, 48.39 %, among others [77].

According to [13], to avoid flicker, the changes in brightness must fall within the maximum flickering time period (MFTP), which is defined as the maximum time period over which the light intensity can change without the human eye observes it. Lacking a widely accepted flicker value, a frequency greater than 200 Hz (MFTP $<$ 5 ms) is considered as safe. Nevertheless, the preoccupation with high amplitude fluctuations of the optical signals remains, especially in the case when a human being is exposed in a VLC ambient for a long time [29].

3.2 OFDM Modulation Format

To obtain higher data rates, increase spectral efficiency, combat intersymbol interference (ISI) and explore the granularity of its multicarrier nature, orthogonal frequency division multiplexing have been considered for VLC systems [78, 79, 80, 81, 82].

OFDM is a modulation format that transmits a high-speed bit stream into a large quantity of orthogonal subchannels (N_{sc}), normally called data subcarriers [83]. With a symbol duration T_s longer than single-carrier signals to combat ISI, each subcarrier carries low data rates in an overlapped manner. Analog OFDM signals can be represented as

$$x(t) = \sum_{i=-\infty}^{+\infty} \sum_{k=1}^{N_{sc}} X_{k,i} \Pi(t - iT_s) e^{j2\pi(k\Delta_f)t}\,, \tag{3.2}$$

where $X_{k,i}$ represents the complex data symbols on the ith OFDM symbol, $\Pi(t)$ a rectangular pulse-shaping and Δ_f the subcarrier spacing. If T_c is defined as the sample or chip period, then $\Delta_f = 1/(N_{sc}T_c)$ and $T_s = (N_{sc} + N_{CP})T_c$, for N_{CP} the samples of a periodic extension of an OFDM signal, denoted as cyclic prefix (CP), used to virtually eliminate the ISI [84]. Therefore, the sampled version of this kind of multicarrier signals can be written as

$$x(nT_c) = \sum_{i=-\infty}^{+\infty} \sum_{k=1}^{N_{sc}} X_{k,i} e^{j\frac{2\pi kn}{N_{sc}}}\,, \tag{3.3}$$

in which $\Pi(t) = 1$ during the symbol duration T_s and 0 otherwise. It can be seen from Equation (3.3) that an inverse discrete Fourier transform (IDFT) can be used to multiplex the complex data symbols obtained after subcarrier mapping in a multilevel signal constellation. Furthermore, the bandwidth of the confined spectrum of an OFDM signal is approximately given by

$$B_w \approx 2\pi \frac{(N_{sc}+1)}{N_{sc}} \frac{(N_{sc}+N_{CP})}{N_{sc}} R\,, \tag{3.4}$$

for R the system symbol rate [84].

3.3 Constant Envelope OFDM

The main drawback of OFDM-based VLC system is related to the high values of peak-to-average power ratio (PAPR) that increases flicker, which is undesirable for human health. Nonlinear companding, iterative clipping, pilot-assisted symbols and selected mapping are some PAPR reduction methods proposed in the literature [85, 86, 87, 88]. However, the constant envelope transformation technique proposed in [89] and experimentally demonstrated in [90] is promising in VLC systems, not only to overcome nonlinearities, as stated in [91], but also to adapt to the flicker levels required by off-the-shelf LEDs.

CE-OFDM is a modulation format where an electrical carrier is phase modulated by OFDM signals, to reduce the inherit OFDM large PAPR [89, 90]. A complex bandpass CE-OFDM signal can be written as

$$s(t) = Ae^{j\phi(t)}, \tag{3.5}$$

where A is the signal amplitude, $\phi(t)$ is the phase signal during the nt signal interval $nT \leq t < (n+1)T$ and T is the signalling interval duration [92]. A real coefficient CE-OFDM bandpass signal, with PAPR = 3 dB, is generated if

$$\begin{aligned} y(t) &= \Re(Ae^{j\phi(t)}e^{j2\pi f_c t}) = A\cos\left[2\pi f_c t + \phi(t)\right] \\ &= A\cos\left[2\pi f_c t + \theta_n + 2\pi h C_N x(t)\right] \end{aligned} \tag{3.6}$$

where f_c is the carrier frequency, θ_n is the phase memory (when $\theta_n = 0$ the modulation is memoryless), h is referred to as the electrical phase modulation index, and C_N is a constant used to normalize the variance of the message signal. Therefore, the signal root-mean-square (RMS) bandwidth becomes $B_{RMS} = max(2\pi h, 1)B_w$ Hz. More details about this transformation technique can be found in [89] and [90].

3.3.1 Increasing VLC Nonlinearity Tolerance by CE-OFDM

In conventional OFDM based VLC systems, nonlinearity is one of the major concerns, also due to the inherit nonlinear characteristics of the LEDs. Therefore, CE-OFDM signals can also be applied to reduce the impact of LED nonlinearity. To substantiate this observation, we conducted experiments in the preliminary setup depicted in Figure 9, in which OFDM and CE-OFDM signals were propagated in VLC links.

Pseudorandom binary sequences [PRBS = $\log_2(M) \times (2^9 - 1)$] were multiplexed in an 64-IFFT after Hermitian symmetry and QAM subcarrier mapping. The 4.76 Mb/s (4-QAM) and 9.5 Mb/s (16-QAM) signals (centered at 7.5 MHz in a 5 MHz bandwidth) generated using Matlab were loaded into a 2.5 Gsamples/s arbitrary waveform generator after cyclic extension (150 ns for 7.65 μs of signal duration). The signals were amplified and superimposed onto the LED bias current, aiming to increase the LED modulation

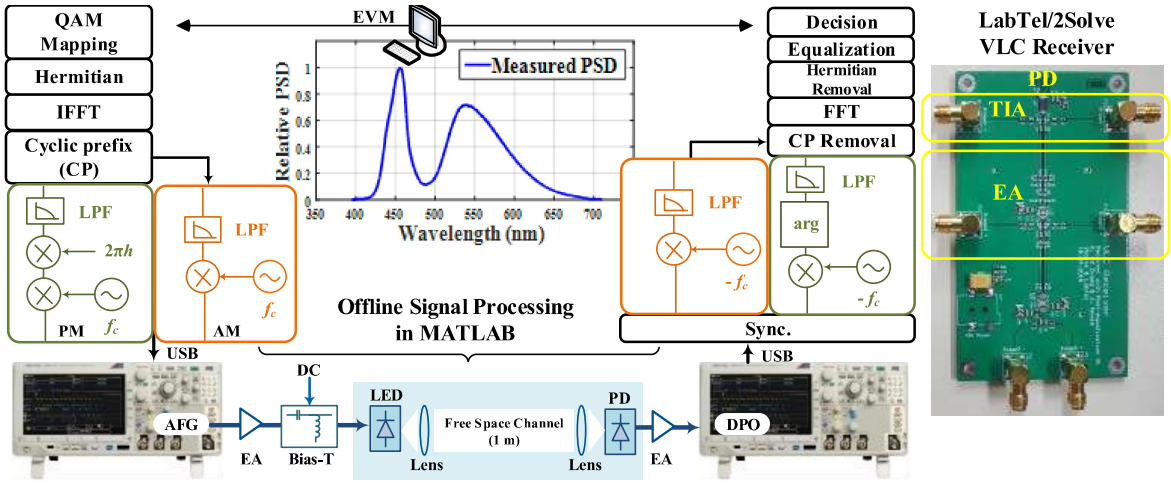

Figure 9 – Experimental setup and insets with PSD and the first manufactured receiver.

depth. The output of the Bias-Tee was directly supplied to the commercial LXML-PWC2 phosphorescent white LED. It should be stressed that a bias voltage of 2.85 was used in all conducted experiments. After free space propagation, supported by bi-convex optical lenses, the VLC signals were detected by a HAMAMATSU S10784 photodiode. The electronic circuit described in Appendix B was built to boost the received multicarrier signals, before offline processing.

As expected, the results presented in Figure 10(a) show that the performance of the CE-OFDM system is dependent on the modulation index h. As an optimal value (see scatterplots shown inset), $2\pi h = 2.2$ was adopted in the rest of the subsequent experiments. Performance evaluations against VLC link length was conducted with conventional OFDM and CE-OFDM formats. Figure 10(b) shows error vector magnitude (EVM)[1] performance comparisons, considering 4 and 16-QAM subcarrier mappings.

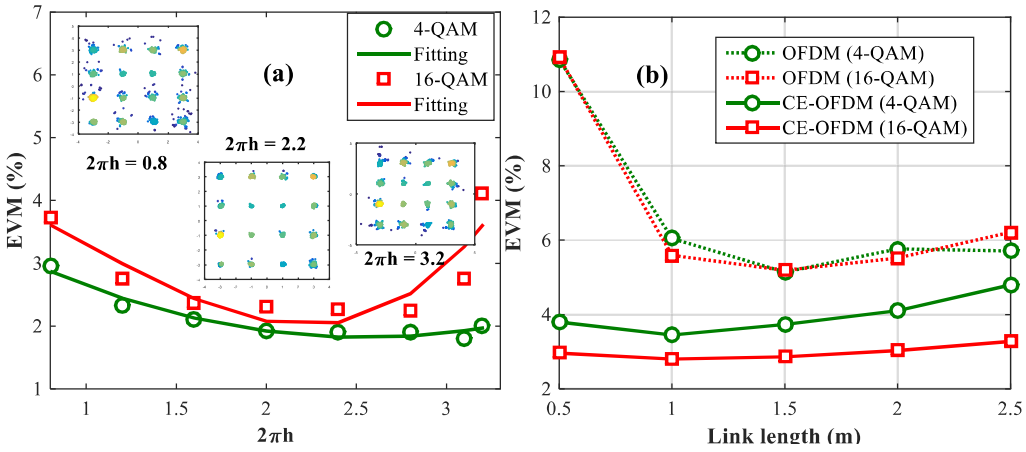

Figure 10 – (a) EVM versus $2\pi h$. (b) EVM against VLC link length.

[1] See Reference [93] for details on the EVM metric.

Figure 10(b) shows that, at 50 cm, conventional OFDM is strongly affected by signal saturation, due to the amplification stages presented in both transmitter an receiver. Hence, EVM penalties up to 8% were achieved, when compared to the proposed CE-OFDM scheme. After 1.5 m, an almost constant CE-OFDM gain of 3% (5.5 dB) occurred when 16-QAM is used as subcarrier mapping. Disregarding the saturation region, with 4-QAM, the gain decreases from $\approx$ 1.5% at 1.5 m to 0.5% at 2.5 m.

3.3.2 Flicker Adaptation Through CE-OFDM Signals

The apparatus of Figure 9 was also used to show the LED flicker adaptation provided by the transmission of CE-OFDM signals in VLC systems. The experimental results depicted in Figure 11 show a performance comparison between VLC systems with OFDM and CE-OFDM signals. Measured in terms of EVM, the performances were evaluated for different common values of flicker. It should be stressed that the employed values of $F_{\%}$ were pre-defined and, in consequence, the quantities A and B of Equation (3.1) imposed in the generated multicarrier signals.

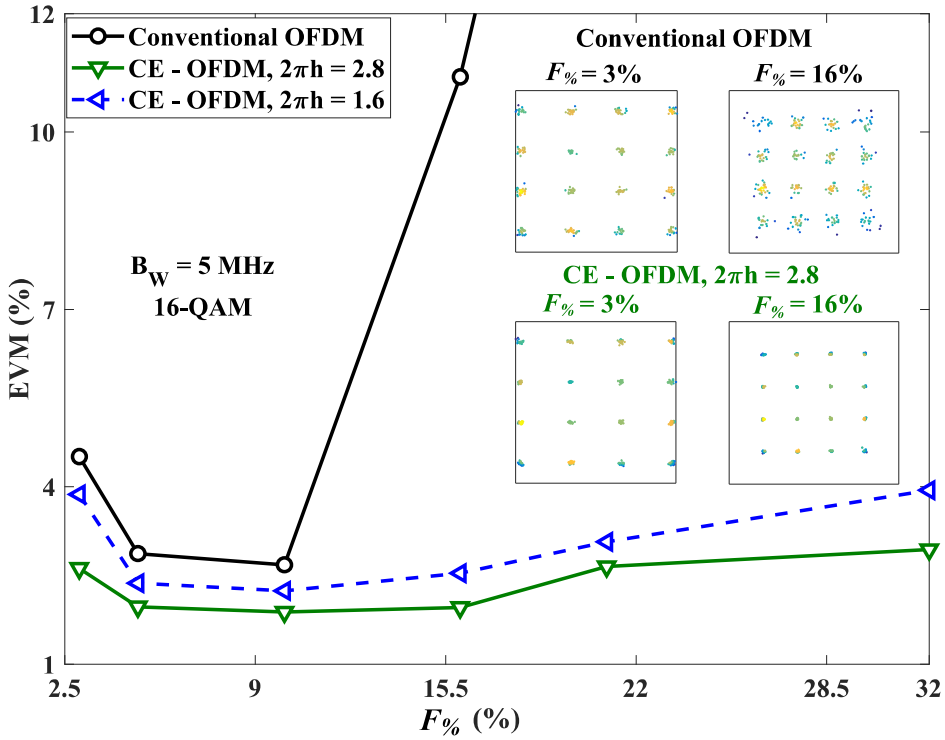

Figure 11 – EVM versus $F\%$ for OFDM and CE-OFDM with $2\pi h = 2.8$ and 1.6.

It is clear from Figure 11 that the system with CE-OFDM signals outperforms the system with conventional OFDM, specially for values of $F_{\%}$ greater than 10 %, which is corroborated by the scatterplots shown inset Figure 11. This is explained by the low value of PAPR provided by CE-OFDM [89, 90].

3.4 OOK with Manchester Coding

The Institute of Electrical and Electronics Engineers (IEEE) proposed the IEEE 802.15.7 standard for short-range OWC using VLC [25]. OOK, variable pulse-position modulation (VPPM) and color-shift keying (CSK) are modulation schemes recommended in the standard, for data rates until 96 Mb/s. Implemented with specific line coding and/or scrambling methods, these schemes are able to mitigate intra-frame and inter-frame flicker [25, 94]. Nevertheless, due to its implementation simplicity and, in consequence, to the cost benefit, this work focuses on the OOK format.

OOK is a type of line coding in which the generated information bits are substituted by pulses [95]. Commonly, the information bit 1 is, during the signaling interval, mapped to positive pulse, whereas the bit 0 is replaced by the absence of a pulse in an unipolar signal formulation, or by a negative pulse if bipolar signal streams are required. The simplicity of this mapping process is requested in low cost applications, such as the one attended in the present work.

Several formation laws can be used during the design of the pulses. The Manchester coding is one of the most employed due to the facilities it provides in clock recovering, while it avoids long sequences of both bits one and zero [95]. The rule that stipulates a positive pulse transition, in the middle of the duration of bit 1, and the opposite to bit 0, was adopted in this work.

3.4.1 System Model

Figure 12 shows the block diagram of the numerical model used to simulate and evaluate the performance of a OOK-based VLC system through AWGN channels. Pseudorandom binary sequences (PRBS) x_k are generated for symbol mapping via Manchester codification [96]. The symbols are then up-sampled and in sequence pulse shaped with, for the sake of simplicity, rectangular pulses, resulting in $s_k(nT)$ modulated symbols.

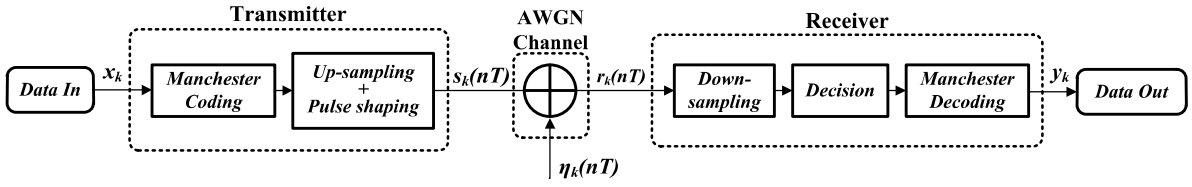

Figure 12 – The OOK numerical model used in the simulations.

It is worth noting that zero mean Gaussian noise $n_k(nT)$ is added through the AWGN channel model. The received OOK signals $r_k(nT)$ are then downsampled, before a symbol recovery decision based on the average integrated signal levels. Manchester decoding can be executed by detection of one of the symbol period halves, leading to a y_k data stream.

Figure 13 shows part of the received pulse streams codified with with Manchester rules. The signals depicted in Figure 13(a) were received without additive Gaussian noise, whereas the ones shown in Figure 13(b) were corrupted by AWGN according to a signal-to-noise ratio (SNR) denoted in terms of energy per bit to noise power spectral density ratio $E_b/N_0 = 11$ dB.

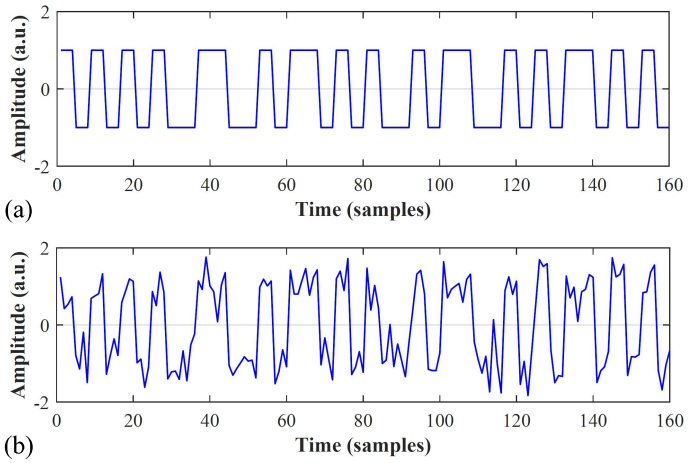

Figure 13 – Received signals. (a) Without noise, (b) with AWGN at $E_b/N_0 = 11$ dB.

3.4.2 Model Validation Through Numerical Simulations

A performance evaluation in terms of bit-error-rate against E_b/N_0 was conducted in order to validate the numerical model, comparing the simulation results with the values provided by a BER closed-form. Figure 14 shows the performance comparison, considering an AWGN channel. The theoretical BER expression used in the comparison is given by

$$\text{BER} = \frac{1}{2} erfc\left(\frac{E_b}{N_0}\right), \tag{3.7}$$

for $erfc$ the complementary error function [69]. The agreement between the simulations and the analytical results validates the numerical mode.

It can be seen from Figure 14 that a BER $= 10^{-3}$ is achieved with an $E_b/N_0 \approx 6.8$ dB, whereas for a BER $= 10^{-6}$ this value increases to ≈ 11 dB. Figure 15 illustrates an eye-diagram obtained with Manchester signals corrupted with AWGN at $E_b/N_0 = 11$ dB. The reasonably open eyes announces a good system performance.

3.5 Estimating the BER and the EOP Metrics from Eye-Diagrams

A performance investigation in which the BER is evaluated by counting the number of different bits between transmitted and received bits can become prohibitive if the communication scenario is extremely favorable. This kind of scenario belongs to the situation where the eye-diagram is well opened, demanding an estimation of the SNR

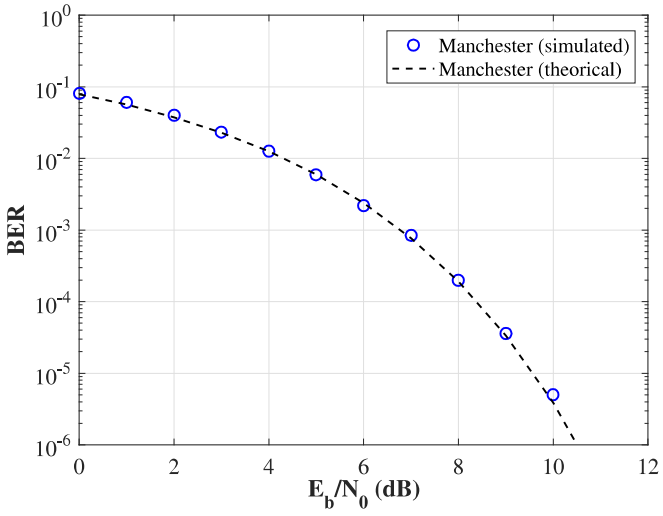

Figure 14 – Numerical and analytical BER versus E_b/N_0 of the Manchester based system.

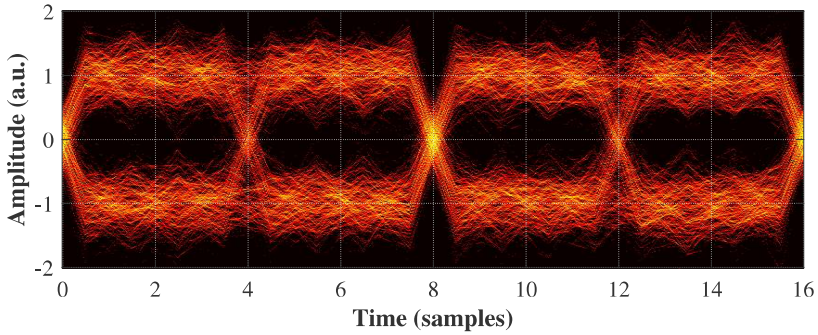

Figure 15 – Simulated Manchester eye-diagram with E_b/N_0 of 11 dB.

through the mean and the standard deviation values of an histogram obtained from the discrete levels of eye-diagrams. In this case, the SNR in dB can be estimated using

$$\text{SNR} = 20 \times \log_{10}\left(\frac{\mu_1 - \mu_0}{\sigma_1 + \sigma_0}\right), \tag{3.8}$$

where μ_0, μ_1, and σ_0 and σ_1 are means and standard deviations of the Gaussian probability density functions (pdfs) of the signal levels that represents bits "0" and "1", respectively [97]. Therefore, in case of Manchester signals, the BER can be estimated as

$$\text{BER} = \frac{1}{2}\left[erfc\left(\frac{|\mu_1 - V_{th}|}{\sqrt{2\sigma_1}}\right) + erfc\left(\frac{|\mu_0 - V_{th}|}{\sqrt{2\sigma_0}}\right)\right], \tag{3.9}$$

for V_{th} a threshold voltage. In this case, it is assumed that the pdf of received signal levels follow a Gaussian distribution, thus enabling a fast calculation of BER values by using the $erfc$.

The quality factor Q is another common measure used to assess the system performance. However, instead of using the mean and standard deviation values of the histograms, it uses the mean and standard deviation values estimated using the dual-Dirac method (see

details of dual-Dirac in [98]). The Q values can be calculated from μ_0, μ_1 and σ_0, σ_1 as follows

$$Q = \frac{\mu_1 - \mu_0}{\sigma_1 + \sigma_0}. \tag{3.10}$$

The BER can be obtained from the Q factor by

$$\text{BER} = \frac{1}{2} erfc\left(\frac{Q}{\sqrt{2}}\right). \tag{3.11}$$

The SNR parameter is a time-averaged indicator used most effectively when noise is the main degrading factor of a system performance. However, when the performance of communication systems is degraded by ISI distortions and nonlinearities in general, it becomes less accurate because the popular assumption that pdf of the received signal levels follows a Gaussian distribution is not suitable. In contrast, waveform distortions are taken into account by using the eye-opening (EO) metric [97]. The EO is determined from the difference between the "mark" and "space" levels. In addition, the eye opening penalty is the penalty of an EO, when compared to a reference EO. This reference EO is usually obtained from a back-to-back configuration, when signal waveforms are not distorted at all. In logarithmic scale, the EOP is normally given by

$$\text{EOP} = 10 \times \log_{10}\left(\frac{EO_{ref}}{EO_{rec}}\right), \tag{3.12}$$

in which EO_{ref} is the eye height, the difference between the positive and negative levels of a reference signal, and EO_{rec} is the eye opening amplitude of the received signal [97]. EO and EOP metrics are useful for noise-free systems as they provide a good measure for pulse distortions. If the distortions are dominated by noise, their calculations become less precise. Moreover, it should be stressed that the accuracy of EO and EOP calculations rely on the sampling instance. Detected pulses are usually sampled in the middle of the eye diagrams where the EO is the widest. Figure 16 depicts an eye-diagram overview showing different kind of signal distortions.

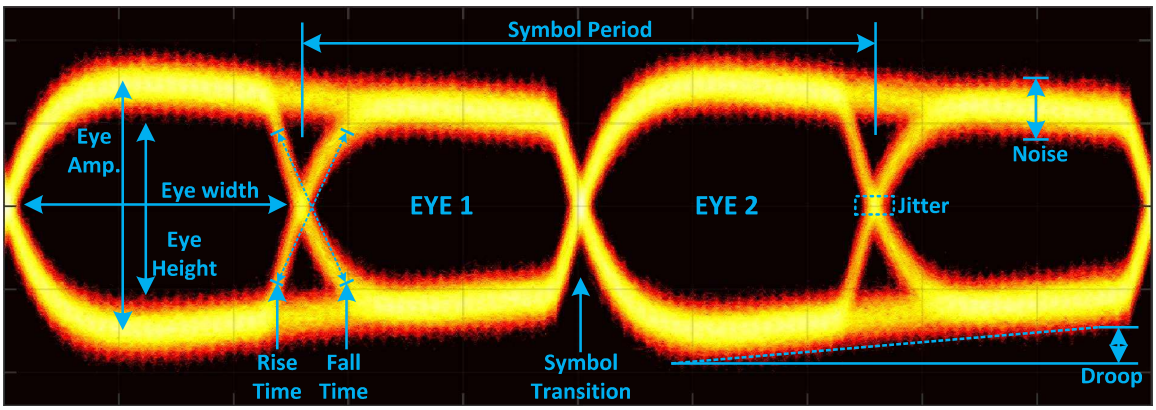

Figure 16 – Eye diagram overview.

An eye-diagram shows a range of effects and signal pattern behaviours from which amplitude and time measurements can be obtained. As shown in Figure 16, the eye height can be derived from the inner amplitudes of both signal levels and used for the EOP metric. It also displays the rise and fall times provoked by the systems capacitance, influencing especially the higher frequencies. The droop phenomenon appears especially at lower frequencies due to the input coupling capacitance. Furthermore, the symbol period of the Manchester symbol with transition can be observed. The two eyes depicted in Figure 16 demonstrate distinct eye amplitudes caused by the droop effect. The illustrated timing variance or jitter can become crucial in low dimming schemes. Because the likelihood the aforementioned distortion effects can arise in the application of this work, the EOP metric supported by eye diagrams can be helpful in the system parameterization.

4 System Design and Characterization

To reach the desired well function of the optical wireless communication system, all components must be studied thoroughly. Moreover, the system characterization in both electrical an optical back-to-back (B2B) should be measured to guide the system design. Thus, the chosen elements of the system and their characterization are described in this Chapter. The characterizations are important since the devices might present different characteristics than the ones displayed in their technical specifications, leading to unexpected functionality.

The chapter begins by displaying a general block diagram of the evaluated VLC system, followed by the characterization of the key components present in the transmitter, the optical channel and the receiver. Then, the electrical and optical B2B characterization are presented and discussed.

4.1 System Block Diagram

Figure 17 depicts a block diagram of the setup prepared to experimentally demonstrate the robustness of the proposed VLC system. The OOK signals, generated using Matlab, are loaded into a 250 MSamples/s arbitrary function generator (AFG), used as digital-to-analog converter (DAC). The analog signals available at the AFG output are amplified and superimposed onto an LED bias current, aiming to provide non-negative amplitudes. The output of the Bias-Tee was directly supplied to a commercial white LED.

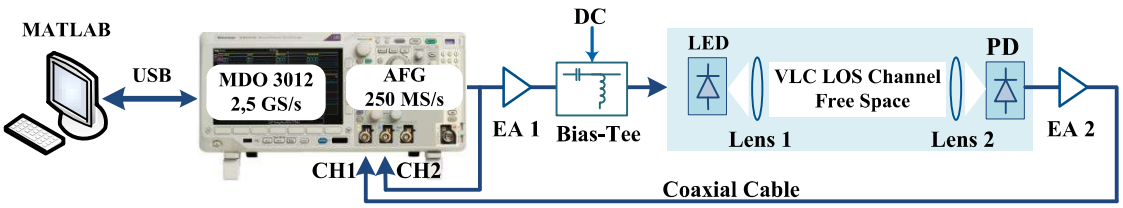

Figure 17 – Block-diagram of the implemented VLC system. EA: electrical amplifier, DC: direct current, PD: photodiode.

After propagation through the optical wireless channel, supported by bi-convex optical lenses, the VLC signals are detected by a photoreceiver, before analog-to-digital conversion (ADC) by a 2.5 GSamples/s mixed domain oscilloscope (MDO). The system performances are offline measured via Matlab.

4.1.1 The Employed Amplifier

In order to amplify the analog signals available at the AFG output, the SHF 100 AP device depicted in Figure 18(a) was used, also due to its availability in the laboratory [99]. It is a low noise broadband RF amplifier, with an operating bandwidth ranging from 30 kHz to 25 GHz, a 19 dB of gain, a maximum input power around 4 dBm, and a maximum peak-to-peak input voltage equals to 1V.

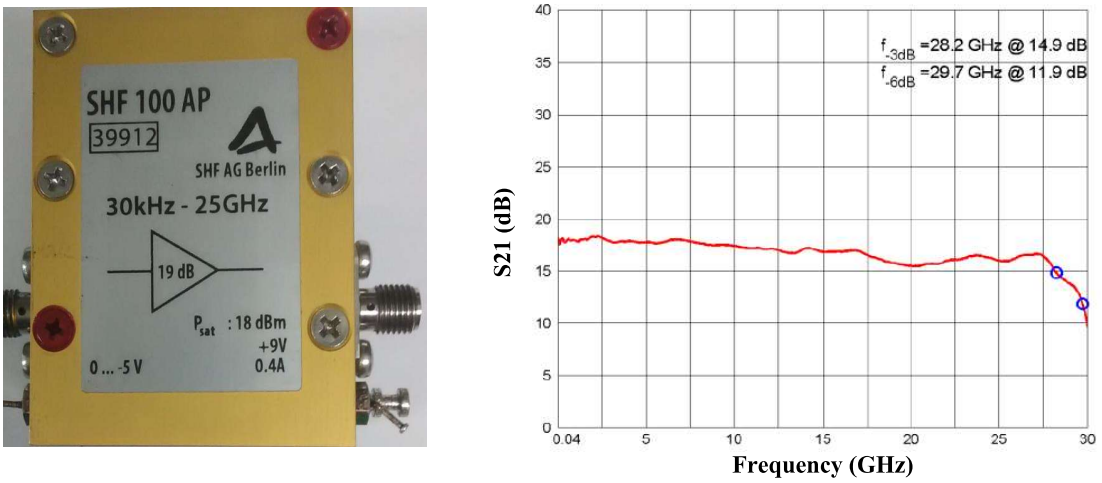

(a) (b)

Figure 18 – (a) A photo of the amplifier. (b) The frequency response taken from its datasheet.

The amplifier was supplied with a positive voltage of approximately +9 V, and its gain can be adjusted by applying a voltage between 0 to −5 V. The frequency response shown in Figure 18(b) illustrates the wide-band characteristic of this electronic device.

4.1.2 The Bias-Tee used to Guarantee Non-negative Signals

To directly modulate the the LED, the RF signals from the AFG needs to be combined with the direct current that drives the LED. This is mandatory because the amplitudes of the optical modulated signals need to be non-negatives. For this purpose, the Bias-Tee from the manufacturer Picosecond Pulse Labs (Model 5575A) was used. Figure 19 shows an image of this device.

Among its main features, the ones that stand out are the bandwidth at - 3 dB (which extends from 10 kHz to 12 GHz), a low rise time of 30 ps, a maximum direct current equals to 500 mA, a 0.6 Ω resistance and a core saturation that limits the low frequency response for currents above 20 mA.

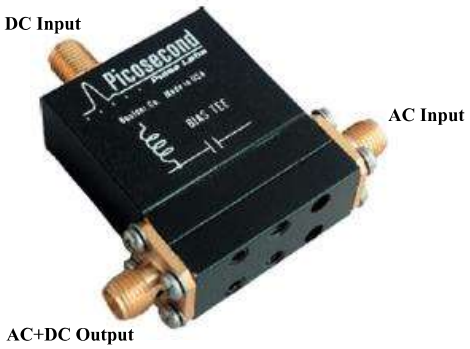

Figure 19 – An image of the used Bias-Tee.

4.1.3 The Manufactured Transmitter

The optical transmitter is an essential component in a VLC system. The commercially LumiLED LXML-PWC2 phosphorescent white LED, depicted in Figure 20(a), was used to build the PCB prototype shown in Figure 20(b) [99]. After the manufacturing process, it was necessary to survey some functionally information, such as the optical spectrum, the characteristic curve that shows the dependence of the voltage on its bias current (I-V curve), as well as the luminance against the DC voltage.

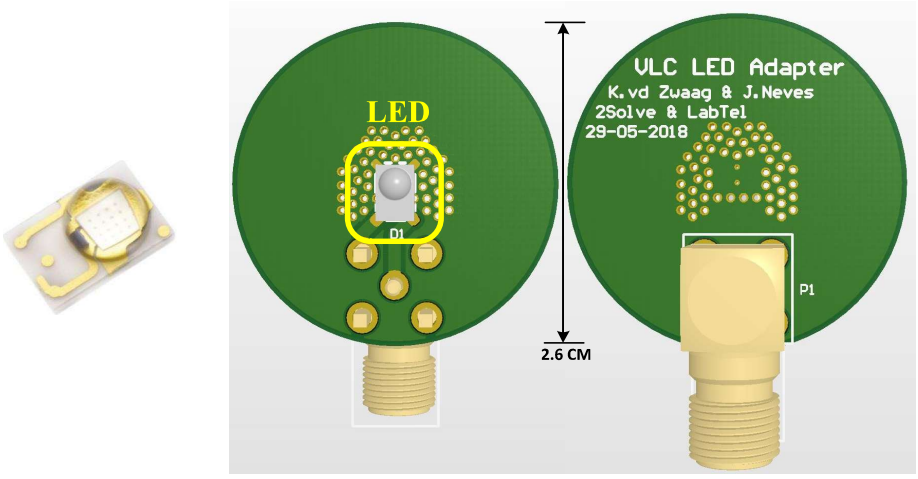

(a) (b)

Figure 20 – (a) The chosen LED. (b) The manufactured transmitter.

The optical spectrum provides information on the radiant intensity of the LED as a function of the wavelength. Figure 21 illustrates the optical spectrum obtained with an Ocean Optics USB2000 spectrometer. According to Figure 21, the optical spectrum has two peaks of radiant intensity. The first occurs in the range of blue light between 450 to 470 nm and the second peak appears in the range of green and yellow light, between 530 to 560 nm. It can be concluded from this measurement that the white LED was manufactured from a blue LED with a phosphor layer used to create the white light.

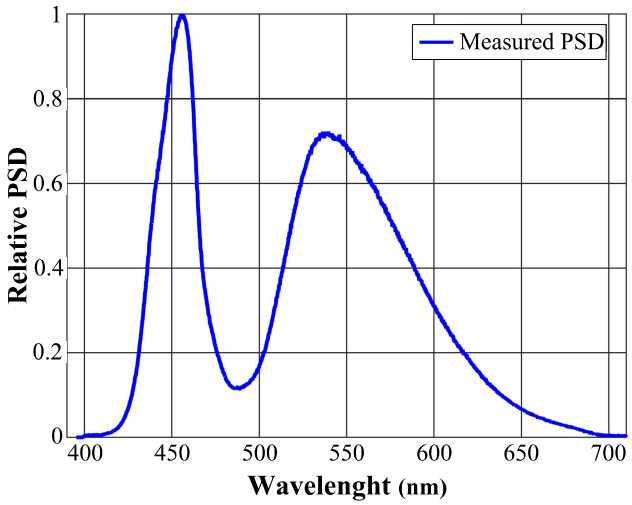

Figure 21 – LED's measured optical spectrum.

To survey the I-V curve of the LED, the DC voltage of a voltage source was manually adjusted to not exceed 3.2 V (value of the LED's datasheet), and the current was adjusted to 0 mA. The current was then varied, and the voltage observed on the source display and a Fluke 87-V multimeter. Figure 22 shows a comparison between the curve provided by the datasheet and the curve measured in different parts of the transmitter.

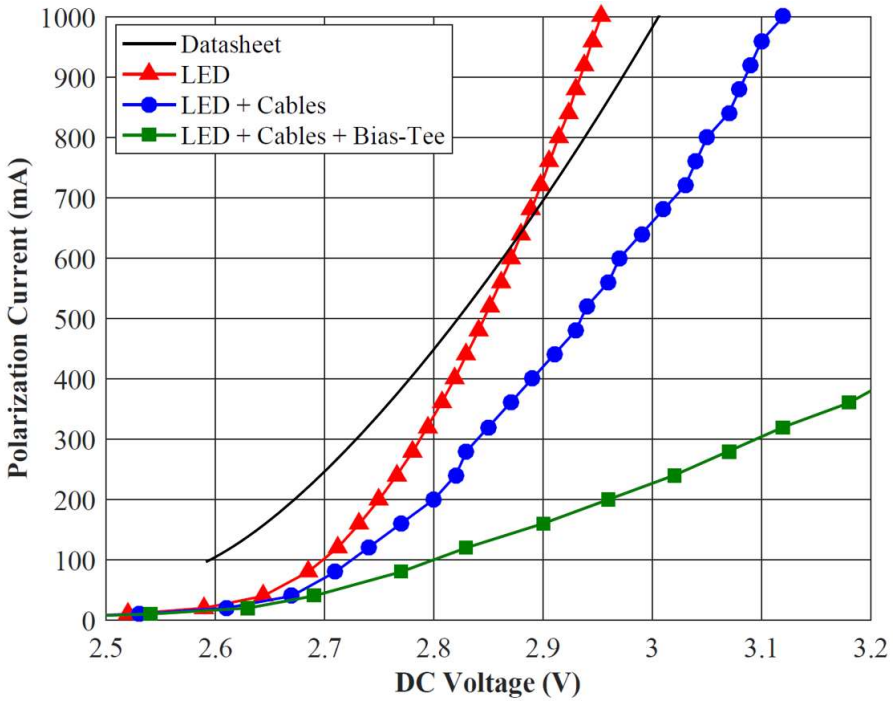

Figure 22 – I-V curves comparison between the datasheet curve and measurements.

It can be observed from Figure 22 that the measurement obtained on the LED terminals is close to the curve provided in the datasheet. The slight differences are due to the different measurement conditions. As expected, the attenuation introduced by the connection cable and the Bias-Tee is prominent.

Illuminance measurements allow the indication of the amount of light within an environment. Figure 23 illustrates the illuminance curves measured as a function of DC voltage, at different positions of a portable luximeter (THDL- 400 model). For each position of the luximeter, the direct voltage of the LED was varied, and the illuminance value observed in its display.

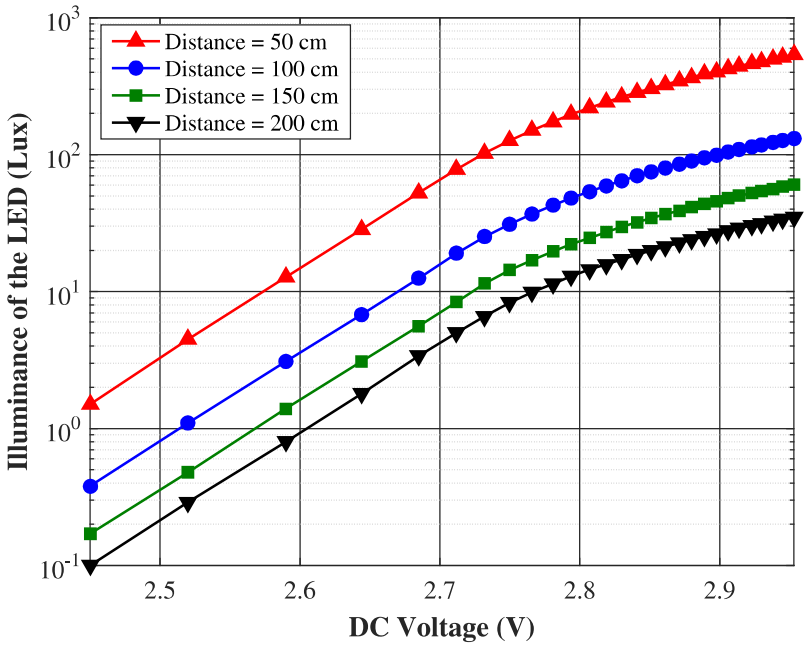

Figure 23 – Illuminance as a function of the LED DC voltage, considering different distances.

Figure 23 shows that, as expected, the light intensity decreases with distance. It can also be observed from Figure 23 that with a DC voltage of $V_{bias} = 2.82$ V, the measured illuminance was 242, 59, 27.2 and 15.8 lux, at 50, 100, 150 and 200 cm, respectively.

4.1.4 The Collimator Lens used in the VLC Channels

The optical wireless channel analyzed in the experiments was configured as an LOS channel, with the emitter and receiver distanced by 1.5 m. Therefore, the power received in the photodetector is approximately constant, since the square of the distance that separates the emitter from the receiver is much larger than the area of photodetection. The signals arrive at the receiver almost at the same time, which means that multipath phenomenon is practically negligible.

To guarantee the LOS peculiarity, two biconvex glass lenses from the PHYWE manufacturer were used to collimate the light beam. These lenses exhibit convergent behavior, which means that a ray that falls parallel to the lens axis refracts on the focus, and a ray that passes through the focus refracts parallel to the axis. The transmitter lens has a focal

length of + 100 mm (Model 41734.2E), while the lens of the receiver has a focal distance of + 50 mm (Model 41734.1E).

4.1.5 The Designed and Manufactured Optical Receiver

The PIN photodiode is one of the main components of the photodetection system, as it is responsible for converting the signal from the optical to the electrical domain. The photodetection system designed and manufactured by researchers from LabTel and 2SOLVE to detect and processes the optical signals from the VLC channel is shown in Figure 24. The main parameters of this system are summarized in Table 3.

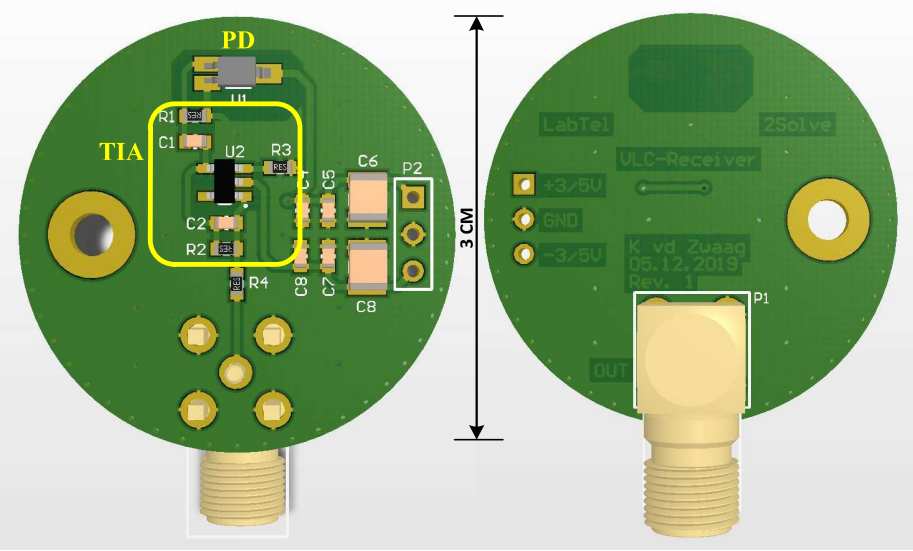

Figure 24 – The designed and manufactured photodetection system.

Table 3 – Main parameters of the photodetection system.

Parameters	**Value**
Spectrum range λ (nm)	380 a 1100
Peak λ employed LED (nm)	870 (R_λ = 0.65 (A/W))
R_λ (A/W)	0.23 (λ = 460 nm) e 0.35 (λ = 530 nm)
Dark current (nA)	1
Capacitance (pF)	4.5
Bandwidth (MHz)	100 (λ = 850 nm)
Radiant sensitive area (mm^2)	1

The PIN used in the first stage of the photodetection system is the OSRAM PIN SFH2400-Z photodiode. The second stage consists of a modified transimpedance amplifier (TIA) with DC-cancellation, used to convert the photocurrent generated by the PIN into a

voltage signal and thereafter amplify it. The employed TIA configuration based on the operational amplifier LMH6629 has a bandwidth of 100 MHz and a gain of 1.8 kΩ. In some cases a third stage with amplification and filtering is desired, although the output voltage of the used setup was sufficient. Additional information about the photodetection system can be found in Appendix B.

4.2 Measurement of the Electrical B2B Frequency Response

To create analog RF signals through the AFG and to recover the digital signals using the MDO, the Tektronix's MDO3012 digital oscilloscope was used. The attenuation profile of the pair AFG + MDO must be outlined in order to assist the identification of the optical limitations. Hence, to characterize the frequency response of this pair, the experimental setup illustrated in Figure 25(a) was prepared, and denominated as electrical B2B because the AFG output was directly connected to the MDO3012 oscilloscope. A frequency scanning was done in Matlab with a variable sine-wave frequency, considering an initial frequency of 1 Hz and a final frequency of 50 MHz.

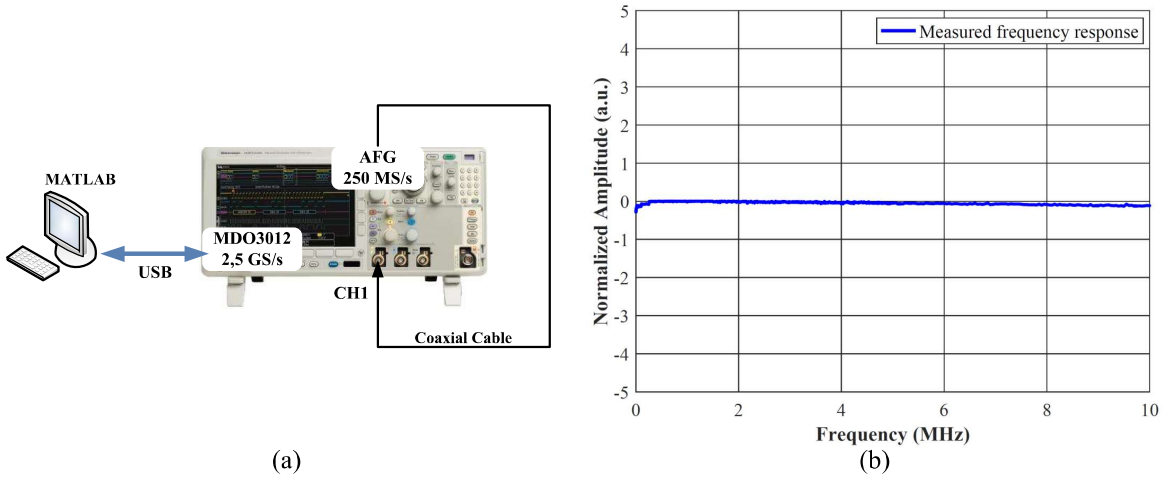

Figure 25 – (a) Setup used in the electrical B2B frequency response measurement. (b) The measured frequency response.

Before scanning, to avoid abnormal offsets or other effects, the oscilloscope was calibrated by its internal routine and both AFG output and MDO input were paired at 50 Ω impedance. The peak amplitude in the frequency domain of each captured sine was stored to generate the frequency response illustrated in Figure 25(b). An almost flat frequency response can be verified in Figure 25(b).

4.3 Measurement of the Optical Frequency Response

Normally, the frequency response of a white LED is modeled as a low-pass filter with a cutoff frequency limited to few MHz [100]. Because this limitation is perfectly perceived in

a frequency response measurement, the apparatus depicted in Figure 26 was prepared. An Anritsu's MS2038C network analyzer was utilized to obtain the frequency response of the VLC system, after a proper parameterization and calibration. It should be stressed that the parameter S_{21} was captured, which represents the profile of the amplitude characteristic of the VLC transfer function, respecting the intensity that can saturate the photodiode.

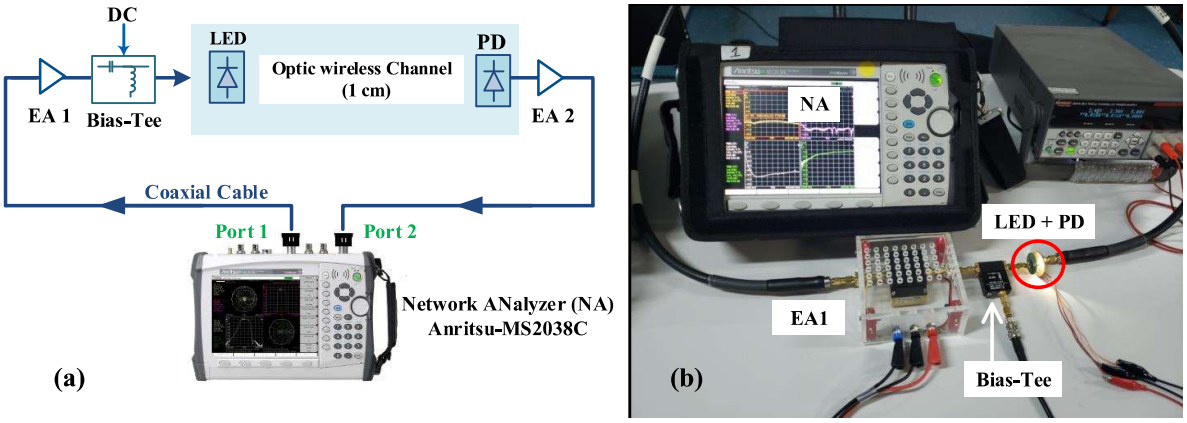

Figure 26 – (a) Experimental configuration used to characterize the VLC system. (b) A photo of the setup emphasizing the miniaturization of the transceivers.

The above-mentioned low-pass characteristic is clearly shown in Figure 27, demonstrating that, indeed, the LED represents the main limitation of the system in terms of bandwidth. Nevertheless, it is important to notice that in the application addressed in this work, this is not the major issue.

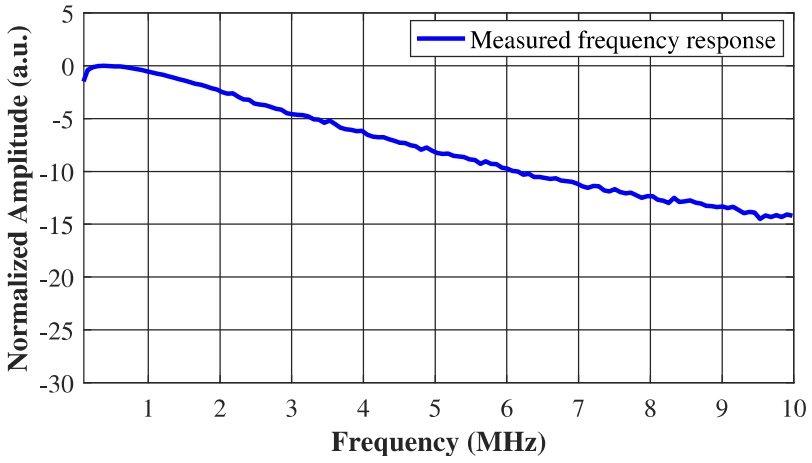

Figure 27 – Measured frequency response of the evaluated VLC system.

It can be seen in Figure 27 that the 3 dB bandwidth of the VLC system is limited to 2.4 MHz. However, if pre-emphasis and/or pos-equalization techniques are implemented in the systems, at a cost of system complexity increases, a bandwidth around 8 and even 10 MHz can be achieved.

5 Experimental Results

To verify the performance of the VLC system arranged with the components discussed in the previous Chapter, various impactful aspects were experimentally tested. This Chapter initially shows the complete system configuration, as well as the form and distribution of the signal eye levels used as reference in the measurements, followed by an impact evaluation of the LED polarization current (I_{DC}) on signal nonlinearities and EOP. Furthermore, the effect of distance and frequency on the system performance are exposed. Last, but not least, the illuminance levels for human well-being and a full demonstration with a multi-parametric monitor as healthcare equipment are carried out to examine the feasibility of the evaluated VLC system.

5.1 System Configuration

Before the exhaustive experimental study, the equipment were calibrated, configured and stabilized. To ensure stable readings, a delay was implemented due to oscilloscopes settling time. It is worth noting that, due to impedance mismatch, distortion appeared at certain frequencies of the B2B received signals. The VLC experiment incorporates adjustment of the channel distance, the signal frequency and the LED polarization current. To resemble diverse conditions, LOS channel lengths of 30 cm to 15 m were established and data transmission rates of 250 kbps up to 10 Mbps were covered. Furthermore, the LED drive current varied among $0-800$ mA to complete a survey that displays the system optimum performance areas. To establish an EOP value used as reference, a normalization process was performed by capturing the peak-to-peak amplitude in a 20 % window in the middle of the pulse. The received signal amplitude was determined and normalized based on peak-to-peak measurement. Table 4 summarizes the main parameters used in the experiments.

Table 4 – Main parameters of the system configuration.

Parameters	**Value**
LOS channel length (m)	0.3 to 15
Data transmission rate (Mbps)	0.25 to 10
LED drive current I_{DC} (mA)	10 to 800
LED modulation current I_{SP} (mA)	400
Superimposed Manchester symbols per eye diagram	9950

Figure 28 shows examples of 1 MHz Manchester signals, upsampled at a rate equal to 8 samples per symbol using Matlab. It can be verified from Figure 28(a) that the symbol duration of the signals employed in the experiments is 1 μs, and long sequences of zeros and ones are prevented by the half-bit transition, that facilitates data synchronization at the receiver. Figure 28(b) shows slight overshoot and undershoot (ringing effect) in the signals received in the B2B configuration. Higher frequencies encountered as well other effects that were related to impedance impairment.

A received signal measured in the integral VLC setup is depicted in Figure 28(c). The low-pass smoothing characteristic demonstrates that the LED is one of the main system limitations in terms of bandwidth. The other main limitation is caused by the electronics coupling capacitance in attempt to eliminate the DC component. Long sequences of ones and zeros will increase the droop phenomenon and, in worse-case, zero-out the pulse. However, in the application addressed in this work, this is not the primary concern.

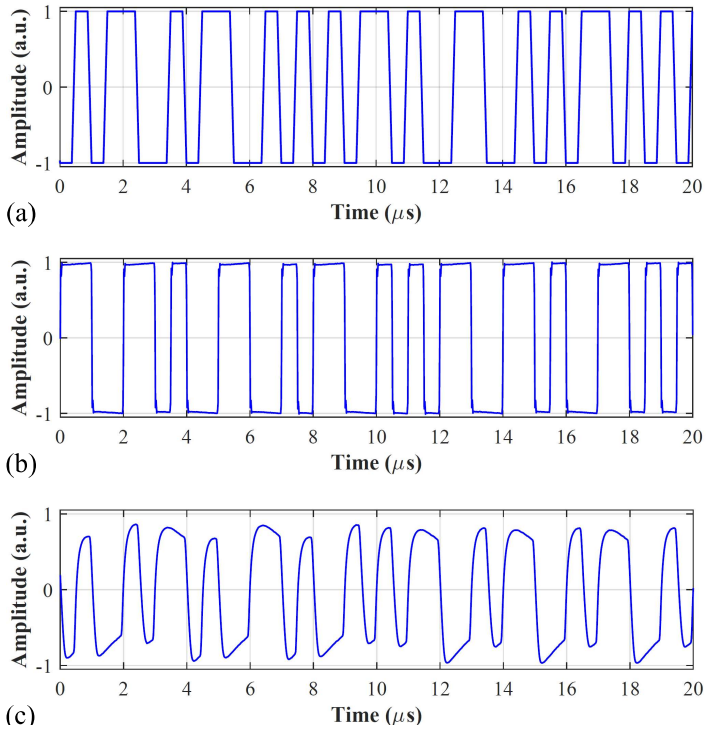

Figure 28 – Examples of 1 MHz Manchester signals. (a) Generated using Matlab. (b) Received in B2B. (c) Measured after propagation over a VLC link of 1.5 m.

As described in section 3.5, the EOP is an appropriate metric to analyze a conditional noiseless system performance, although affected by signal distortions. In this work, the EOP metric is referenced on the B2B eye diagram shown in Figure 29. Every eye diagram in this work consists of 9950 superimposed received symbols, divided into two symbol periods and the Manchester symbol transition in the middle. It can be seen from Figure 29 that a minor ringing effect is present and the horizontal levels tend to rise. The B2B eye diagram depicted in Figure 29 can, nevertheless, be used as a reference.

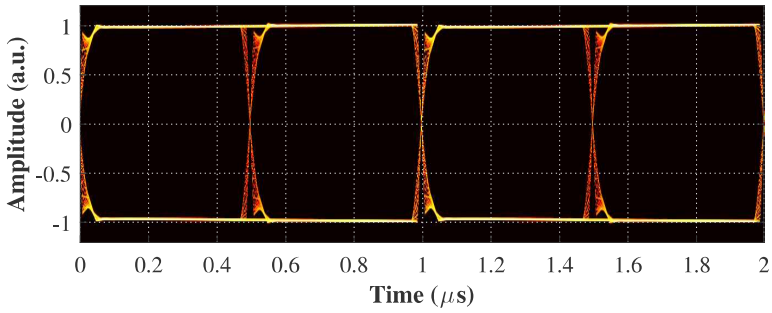

Figure 29 – The 1 MHz Manchester eye-diagram measured in B2B.

5.2 An Eye Diagram Used as Reference in the Measurements

In addition, to corroborate the adoption of the eye opening penalty as a metric in the performance evaluations, a VLC link length of 1.5 m and a signal fundamental frequency of 1 MHz were settled. Therefore, the eye diagram shown in Figure 30(a) can be understood as a reference eye diagram for the rest of the measurements. The two main distortions depicted in Figure 30(a) denote system capacitance effects. Firstly exposing the LEDs high frequency limitation on the rising and falling edges, and secondly a droop phenomenon limiting lower frequencies due to coupling capacitance. A deformation, that is caused by saturation of the receiver, elevates the eye crossing amplitude due to unbalanced positive and negative pulse duration.

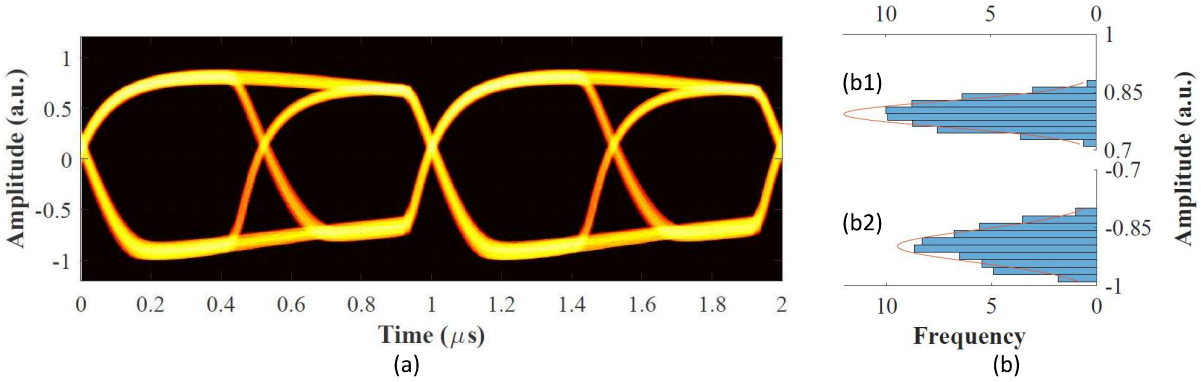

Figure 30 – (a) The eye-diagram of the 1 MHz Manchester signals received after propagation in a VLC link of 1.5 m. (b) Distribution of the signal levels.

On behalf of simplicity, the eye of the right symbol-half shown in Figure 30(a) was outlined in this work, due to the largest signal eye opening. To verify initial EOP results, a sample at 250 μs (the maximum EO_{ref}) and a sample at 360 μs (the maximum EO_{rec}) were considered. As mentioned earlier, a Gaussian distribution of the signal levels is key in the implementation of the EOP metric.

The histograms displayed in Figure 30(b1) and (b2) represent the positive and negative level distributions at the sample intervals. Although the mean of the distribution is shifted

due to nonlinearities, it is possible to conclude that both levels are conform this Gaussian condition. With 1.92 and 1.52 (a.u.) for EO_{ref} and EO_{rec}, respectively, the obtained EOP is 1.02 dB. The signal-to-noise ratio, based on the standard-deviation and signal mean levels, of the received VLC signal, showed 27.01 dB, whereas the BER calculated from this SNR is 4.23×10^{-101}. Because of this so low BER, the EOP metric represents a good choice, in detriment of BER, to exhibit the performance of such relative noiseless VLC system.

5.3 Evaluating the Impact of the LED bias Current

It is straightforward thinking that, taking into account the aforementioned physical limitations, the LED bias current (I_{DC}) plays an important role in the performance of VLC systems. The importance of the I_{DC} parameter is also evident regarding dimming and human health [101]. Nonetheless, performance degradation due to nonlinearities is expected when the bias current boundaries are exploited. The EOP as function of bias current, measured at 1.5 m with a frequency of 1 MHz, is shown in Figure 31. Taking an EOP of 15 dB as a reference penalty, it is possible to observe from Figure 31 that an error-free performance is reached in the wide range of currents between 10 and ≈ 700 mA.

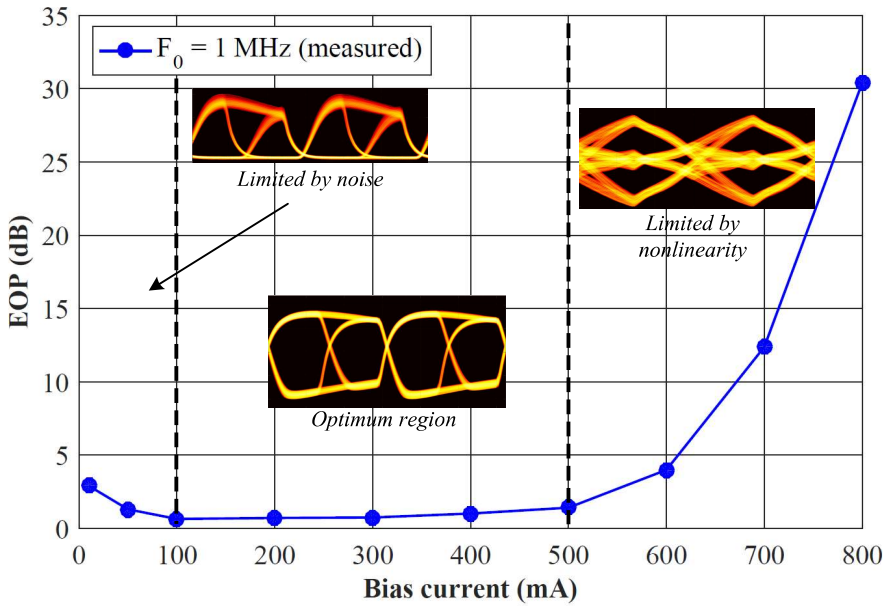

Figure 31 – EOP as a function of the bias current I_{DC} at a distance of 1.5 m and a frequency of 1 MHz. Eye diagrams are shown as inset to emphasize the impact of clipping noise and nonlinearities.

As expected, three performance regions can be established in the measured curve depicted in Figure 31 [90]. In the first, comprising the bias currents between 0 and 100 mA, the system performance is limited by electronic and signal clipping noise [101]. In this case,

the intensity of the signal is reduced, as well as the SNR, increasing thereafter the EOP. This is substantiated by the left eye diagram depicted inset in Figure 31.

An optimum performance region is verified in Figure 31, with the currents adjusted between 100 and 500 mA. The wide open eye-diagram shown in the middle of Figure 31 corroborates with such definition. EOP values of 1.4 dB up to 30.39 dB obtained at 500 and 800 mA, respectively, marks the area where the performance is affected by the system nonlinearities. It should be stressed that these nonlinearities are raised mainly by the transmitter and receiver saturation [102]. The astonishing eye-diagram reproduced in the nonlinear region illustrates the impossibility of bits recovering. The bandwidth limitation of the employed LED also suggests a limit in the fundamental frequency of the Manchester pulses. Figure 32 shows results of a performance analysis that considers the three distinct frequencies 0.5, 1 and 5 MHz. The effects of the system bandwidth and nonlinearities are apparently displayed with the measurements of EOP. These measurements were also executed considering a VLC link of 1.5 m.

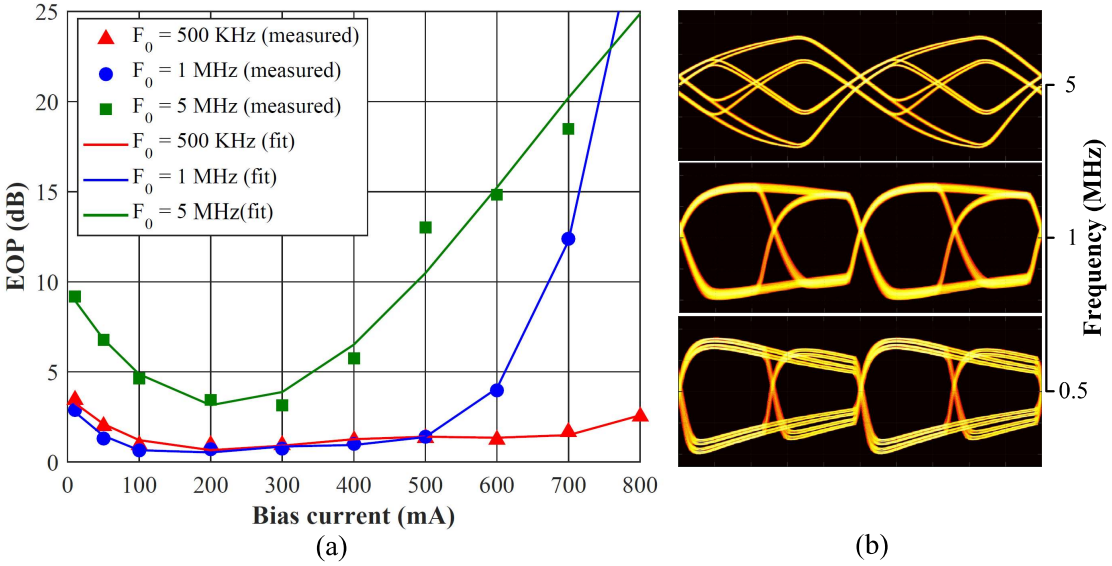

Figure 32 – (a) EOP versus I_{DC} measured with frequencies of 0.5, 1 and 5 MHz, in a link of 1.5 m. (b) Corresponding eye diagrams captured with $I_{DC} = 400$ mA.

Figure 32(a) shows that the system performance degrades with the frequency of the modulation format, especially at higher bias currents. With $I_{DC} = 700$ mA, the measured values of EOP were 1.68, 12.37 and 18.47 dB for frequencies of 0.5, 1 and 5 MHz, respectively. Moreover, a high performance correlation can be observed with the signals generated with the frequencies of 500 kHz and 1 MHz signals, in the range between 0 and 500 mA. Although lower frequencies achieve better EOP at higher bias currents, unsurprisingly, an overall higher penalty appears due to the LED bandwidth limitation. Figure 32(a) presents an EOP increase of 2.42 and 11.6 dB at 300 and 500 mA, respectively, for a 5 MHz signal in comparison to 1 MHz. The limiting bandwidth distortions are also illustrated in the corresponding eye diagrams shown in Figure 32(b), measured with $I_{DC} = 400$ mA.

5.4 Performance Analysis at Different Link Lengths

Another important aspect is the performance of the VLC system over distinct distances. Once adequately developed, this analysis allows a certain degree of freedom when a smartphone and/or a tablet are utilized as opto-electric conversion devices. The impact of link distance in the system performance can be analyzed in Figure 33, considering the three frequencies 500 kHz, 1 MHz and 5 MHz. In this case, the EOP was measured after propagation over link lengths that vary from 30 cm until 15 m, with I_{DC} fixed at 400 mA.

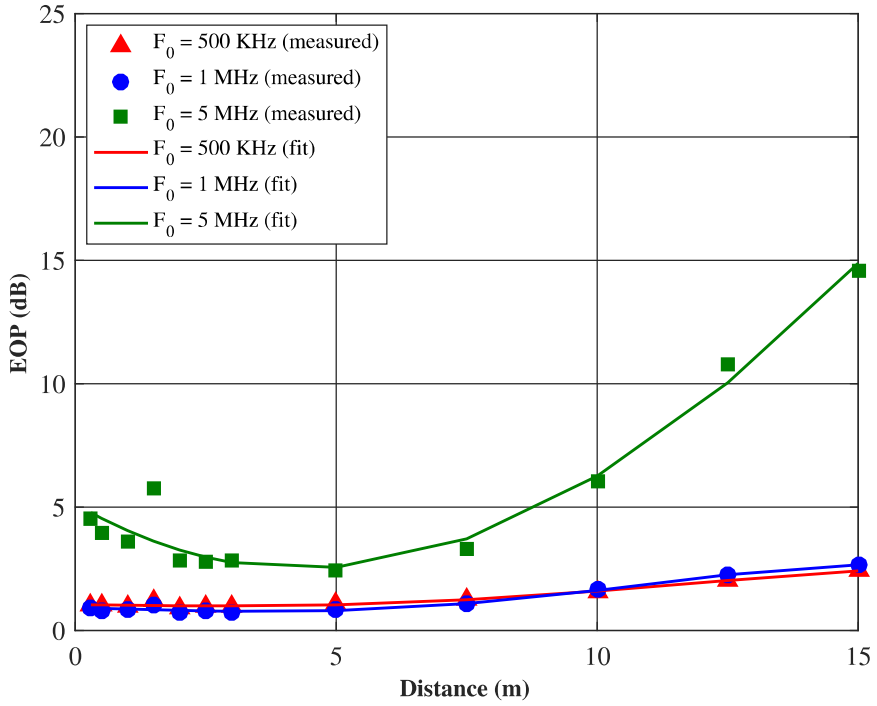

Figure 33 – Measured EOP as a function of the transmission distance with three different frequencies and an LED polarization current of 400 mA.

Figure 33 demonstrates that signals generated with the lower frequencies are less sensitive to distance, as verified with the fact that the performance results of 500 kHz and 1 MHz are nearly superimposed. The measured EOP values for 0.5 and 1 MHz were 1.03 and 0.85 dB at 50 cm, 1.08 and 0.81 dB at 5 m, and 2.41 and 2.66 dB at 15 m, respectively. However, when 5 MHz is the fundamental frequency used in the Manchester signals, performance penalties around 3.14, 1.58 and 11.91 dB were registered at 0.5, 5 and 15 m, respectively, compared to the curve obtained with 1 MHz. Figure 33 also shows that outliers occurred at 1.5 m due to the photoreceiver saturation generated by means of optimum focal point. The first column of Figure 34 confirms this nonlinearity phenomenon that was caused because the system was aligned at this distance, before the followed measurements.

An eye diagram analysis was performed to validate the signal patterns and simultaneously the exploitation of the EOP metric, at various link distances. An overview is shown in Figure 34 with link lengths equal to 1.5, 5 and 15 m, and frequencies of 0.5, 1 and 5 MHz.

As can be seen, shorter distances are impacted by nonlinearity in terms of signal level imbalance caused by the elevated light intensity and, consequently, by receiver saturation. A decrease in SNR is slightly noticeable at 5 m, unlike the significant decrease registered at 15 m, that results in the EOP of 14.57 dB shown in Figure 33. Again, the SNR and the BER metrics remain at 10.67 dB and 6.62×10^{-4}. An interesting fact is that low frequencies show better performance with the second eye, in contrast to the higher frequencies that show better performance with the first, as can be seen in Appendix A. This claim supports the previous decision related to the exploitation of the second eye in the signal detection.

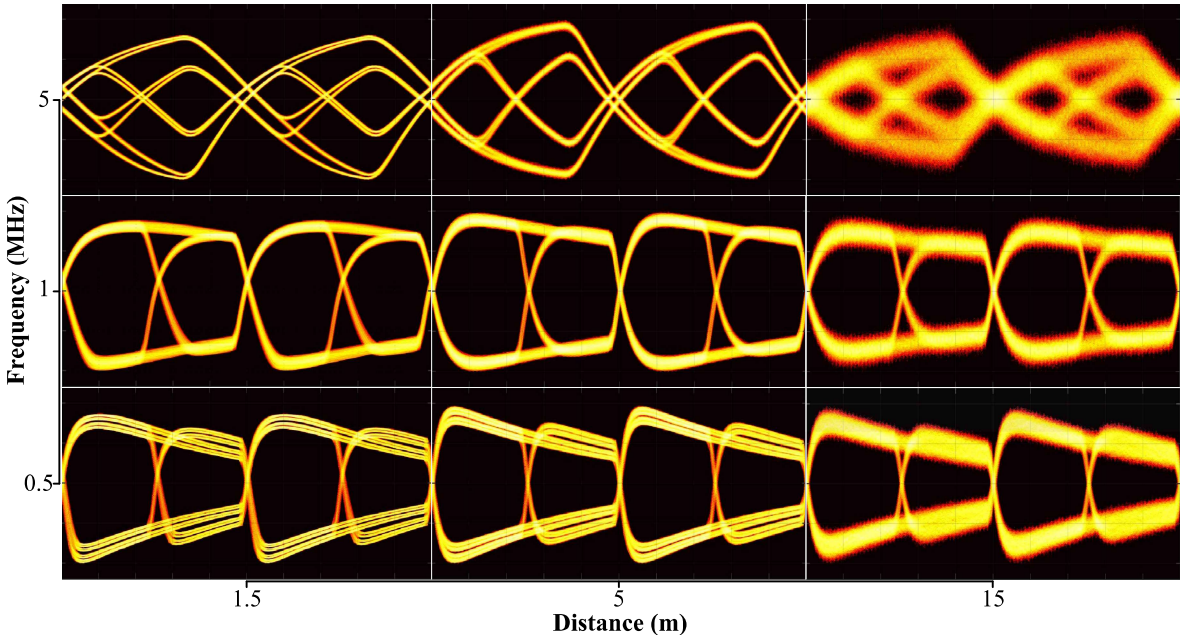

Figure 34 – Eye diagram overview with frequency as a function of the distance, obtained at a bias current of 400 mA.

5.5 Exploring the Systems Optimum Performance

A fixed LED polarisation current was also investigated during the experiments. Although, in practice, the system design for hospital applications is complex, where illuminance and distance constantly differ, robustness is essential. To understand the flexibility of the design, and to actuate in the optimum operating region, a detailed survey was executed. At each distance, the EOP was measured considering various bias currents and frequencies. It should be noticed that, after the above analysis, this work focused on the lower frequencies, due to the nature of the application.

It is clear from Figures 35(a) and 35(b) that, due to high illuminance intensity, all frequencies at distances up to 1.5 m suffer saturation distortions with currents approximately above 500 mA. However, error-free system behaviour is presented at further distances from $\approx$ 10 up to 800 mA, with 0.5 to 3.5 MHz frequencies. As expected, the EOP increases

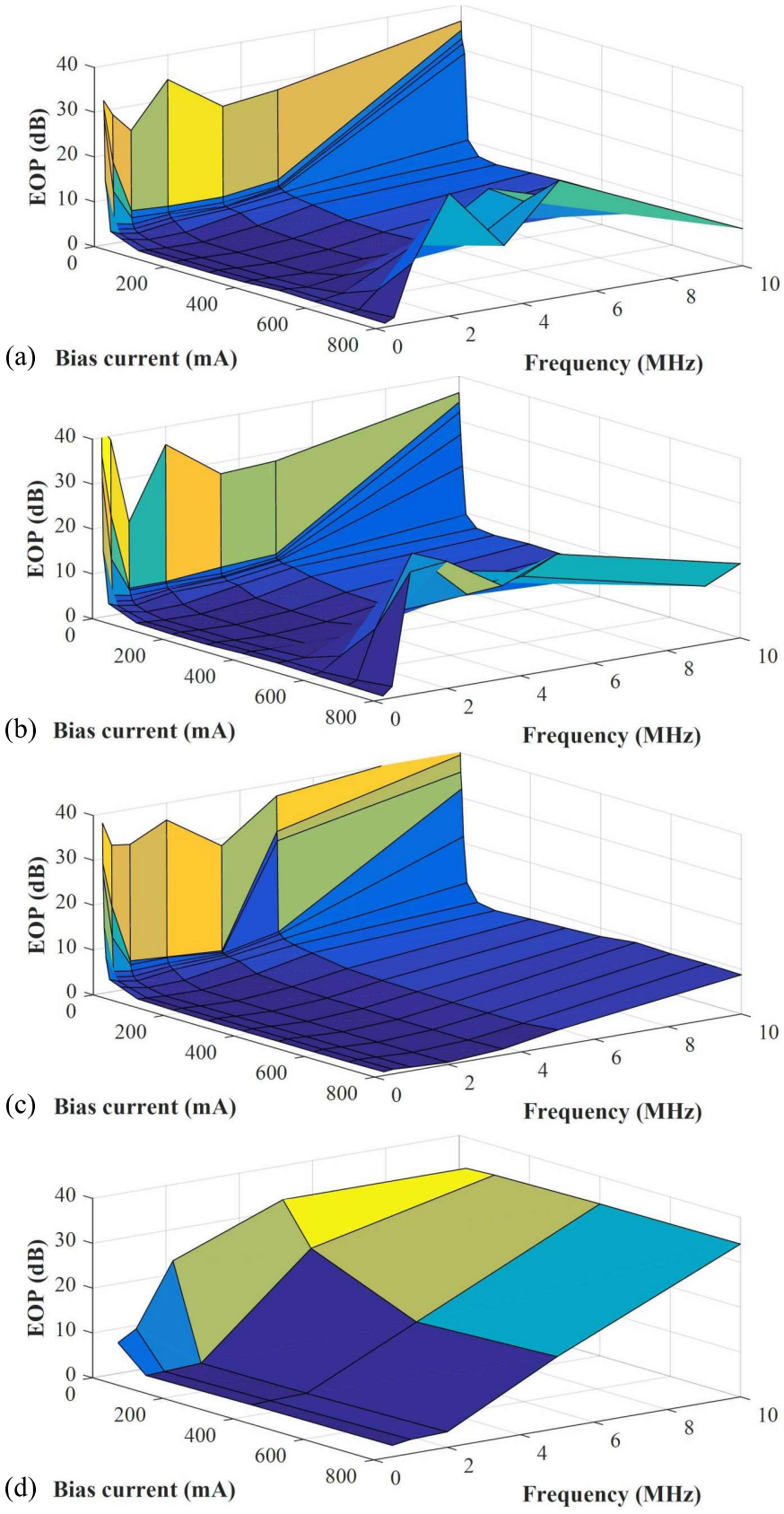

Figure 35 – The EOP as function of both bias current and frequency. (a) At 0.5 m. (b) At 1.5 m. (c) At 3 m. (d) At 15 m.

with frequencies above 3.5 MHz and distances beyond 7.5 m. Nevertheless, a short communication link based on 10 MHz can be achieved with an EOP ranging from 6.27 to 10.69 dB, for VLC link lengths between 0.3 and 5 m.

Typical VLC channels in hospitals can be established directed downwards from the ceiling and, in some cases, directed from walls, which leads to distances between 1 and 3 m. Nevertheless, the results presented in Figure 35(c) and Figure 35(d) prove that the evaluated VLC system can also be applied in relatively long range environments, with a dimming range around 10 up to 700 mA and at a cost of signal frequency reductions.

5.6 Illuminance Susceptibility Survey

Whilst the evaluated VLC system shows a high degree of flexibility, it must comply to some standards, considering that it will be implemented in an intensive care or in a general hospital environment [103]. It can be derived from the standard that the observation/night light at IC and ward environments demand 20 and 5 lux, and general lighting of 200 till 1000 lux, respectively. From this perspective, a research was executed to validate compliance of the complete system with collimators. Figure 36 illustrates an overview of the illuminance measured at the VLC receiver side as function of LED bias current, captured at varies distances through a portable luximeter (THDL- 400 model).

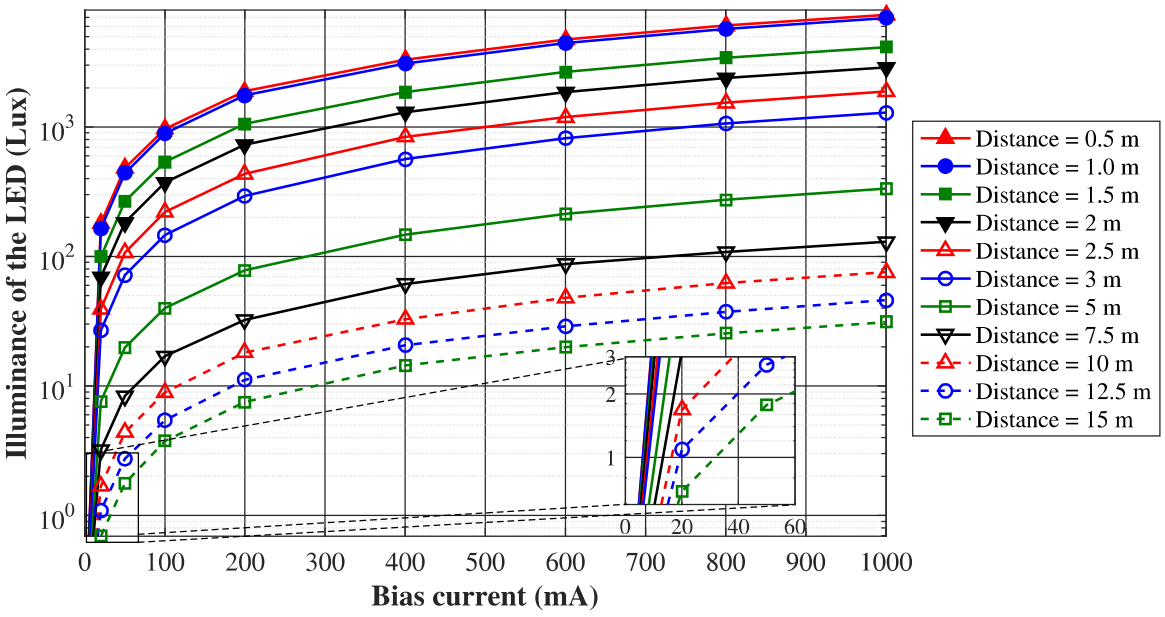

Figure 36 – Illuminance as a function of the LED bias current, considering different distances.

Figure 36 shows that illuminance values between 26.81 and 164.3 lux with 20 mA, and between 1062 and 5730 lux with 800 mA were recorded at distances ranging from 1 to 3 m, respectively. Diverse measurements with values below 20 lux (in particular between 0.69

and 5 lux) are clearly noticed, marking the recommended IC illuminance standard. This also allows the conclusion that the receiver is adequate for such so sensitive environment.

Although the systems lux between 1 and 3 m is high compared to the standard, some minor adjustments at the transmitter can reduce the illuminance. From Figure 23, where the illuminance was measured without collimators, it can be concluded that a luminaire with a more diffuse light addresses this concern. Another solution can be sought in applying an I_{DC} below 10 mA, along with optical modulation index adjustments.

5.7 Experimental Results with the Multi-parameter Monitor

Finally, after all experimental results that proved the feasibility of the prepared VLC system, the developed prototype was examined in a health-care setup. Accordingly, a multi-parametric PRO12 monitor was used as displayed in Figure 37, to resemble a health communication environment. This monitor captures vital parameters, such as heart rate, oxygen saturation, pulse rate, respiration rate, temperature and non-intrusive blood pressure, and utilizes the HL7 protocol for data communication [104]. It should be stressed that HL7 is nowadays the recommend protocol for communication with this kind of multi-parameter monitors. Since the HL7 protocol is limited, the transmitted data was used for trend analysis, like a central monitoring system applied in hospitals. The data acquisition was executed every second over a LAN connection and sent to a local HL7 server, and then prepared for VLC transmission through the evaluated setup. Due to limitations on opening and closing the connection between TekVisa and the oscilloscope, that takes up to 70% of the transmission total time, the VLC refresh-rate was between 1.5 and 2 s.

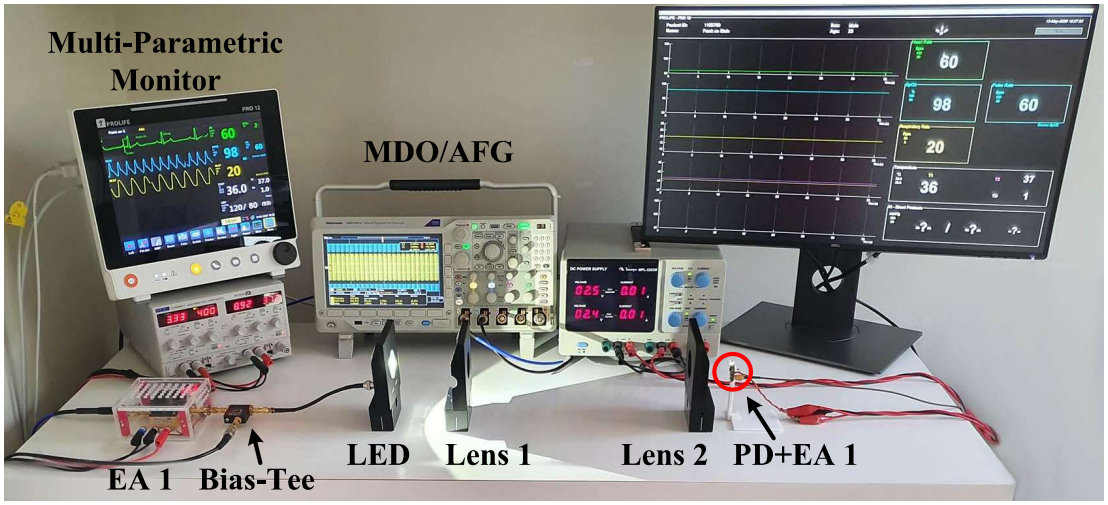

Figure 37 – A photo of the VLC system in an health communication environment with a multi-parametric monitor. EA: electrical amplifier, PD: photodiode.

It is worth noting that the setup depicted in Figure 37 is based on the diagram of Figure 17,

with a multi-parametric meter as addition. In the reception, a simple form of checksum is executed on the data that contains information related to heart rate and respiration rate based on a ECG-measurement. Likewise, an oxygen saturation (SPO_2), a pulse rate based on SPO_2, and a temperature measurement belong to the 1 Hz data string. A non-invasive blood pressure measurement is sent solely, after the execution of a respecting measurement.

It is also important to notice that, despite its absence in Figure 37, the information captured in Matlab was used to generate the OOK signals based on Manchester coding, that served for modulating signals in the optical modulation process. This means that the codified pulses were offline generated using a fundamental frequency of 1 MHz, and the analog signals provided at the output of the AFG modulated the LED. Due to the provision of 420 symbols up-sampled at 8 to 3360 samples in total, the oscilloscopes parameters and settings with a resolution of 10 samples per symbol were achieved and shown in Figure 38.

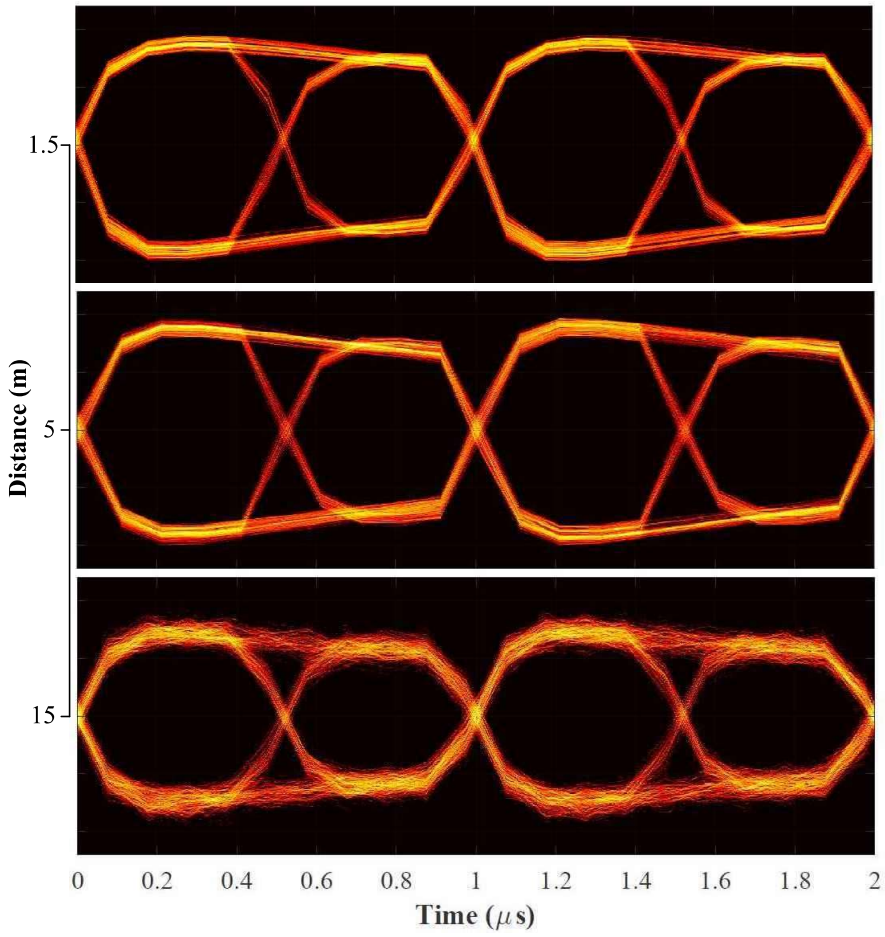

Figure 38 – Eye diagrams of received vital parameters at 1 MHz, 400 mA bias current and link lengths of 1.5, 5 and 15 m.

The captured vital parameters were sent considering an LED polarization current of 400 mA, at VLC distances of 1.5, 5 and 15 m. Figure 38 shows eye diagrams of the received signals with all evaluated distances. As can be observed in Figure 38, the already down-sampled signals at the reception present a slight deviation in the final EOP, although

the obtained results follow the line of earlier experimental results of Figure 33, where 1.02, 0.83 and 2.66 dB were achieved at 1.5, 5 and 15 m, respectively. Results with the multi-parametric monitor provide EOP values equal to 0.89, 0.96 and 2.67 dB at the equivalent distances.

In Figure 39(a), a snapshot of the real-time multi-parametric meter screen is shown. Besides this, Figure 39(b) depicts a screenshot of the HL7 semi-real-time data, measured by the sensors and captured with a graphical interface prepared in Matlab. It can be seen from Figure 39(b) that the measured data was successfully recovered after propagation over a VLC link of 1.5 m. Therefore, these results prove the feasibility of the VLC technology as a robust alternative in intensive care medical environments.

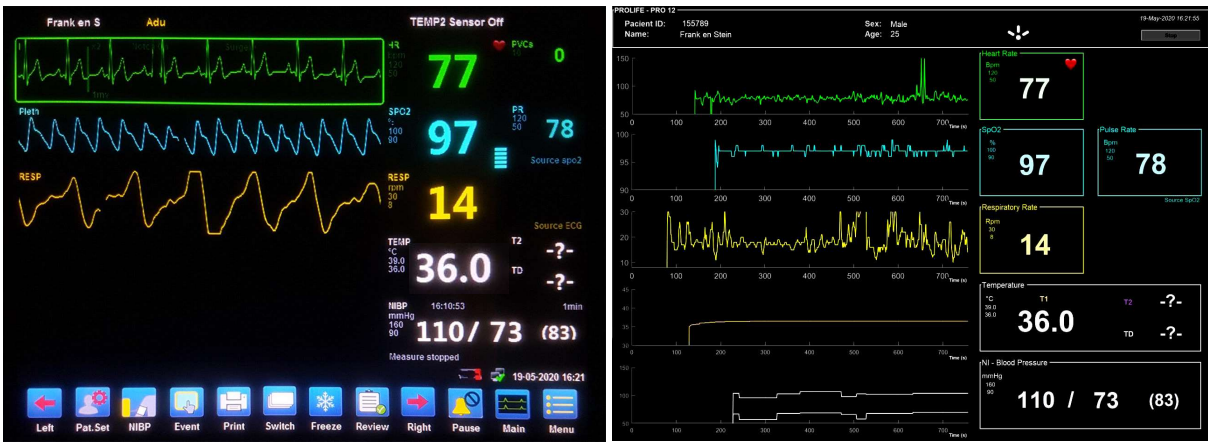

(a) (b)

Figure 39 – Generated and received vital parameters. (a) Data generated in multi-parametric monitor PRO12. (b) Corresponding parameters received in Matlab.

6 Conclusion and Future Works

It is well known that the 5G and beyond of mobile communication networks are emerging as revolutionary technologies supporting, among others, ultra-reliable wireless connectivity for human-oriented and machine-type communications. In this context, optical wireless communication reappeared as a promising technology that can easily, among others, block locally confined interference by physical separators or beam adjustment, avoiding data rate collapses and latency growth. As an OWC solution, visible light communication has emerged as a promising and complementary technology to radio frequency, due to advantages like green technology, unlicensed spectrum, low energy consumption and absence of electromagnetic interference. Allied to this, as a technology that employs light emitting diodes for data transmission, it also ensures the lighting functionality along with the prevention of spreading emerging diseases, allowing its adoption in classified medical environments.

Therefore, a VLC system for application in intensive care medical environments was proposed, designed, characterized and experimentally evaluated in this work. Indeed, numerical and experimental performance assessments show the feasibility of a stable and reliable data connection at different VLC link lengths and light intensities, with a straightforward and low-cost solution based on an on-off keying signal codification. The OOK modulation format was appointed, after a preliminary study of flicker reduction on OFDM-based VLC systems, to accomplish the simplicity requirement established in the system design, as well as to explore light power maximization provided by constant envelope signals. Performance comparisons between analytical and numerical simulation validated the numerical model subsequently used in the offline proof-of-concept experiments. The discerned communication scenario contemplated a line-of-sight propagation channel in a single-input and single-output VLC system.

Two distinct prototypes were developed and merged into an experimental setup, successfully evaluating the proposed proof-of-concept. The former, equipped with specific and costly components, performed well with the OFDM-based schemes, although with limited applicability at lower frequency OOK signals. The latter addressed this limitation with off-the-shelf electronics and a cost reduction from 124$ to 15$ respectively. Regarding an analysis of the system electrical and optical limitations, the experimental results, based on the eye opening penalty metric, show a comprehensive picture of the system performance. The impact of parameters such as the LED bias current, the modulation frequency, the LOS link distance, the signal pattern and the illuminance sensitivity were extensively evaluated. The in-depth study provided a satisfactory understanding of system flexibility

and optimum operating area. Currents above 500 mA at distances up to 1.5 m provoked a degree of saturation nonlinearities. Despite these nonlinearities, extraordinary performance was exhibited at distances beyond, with EOP values ranging from 0.41 to 4.48 dB, frequencies extending from 0.5 to 3.5 MHz and currents between $\approx$ 10 and 800 mA. The increased values of EOP, registered at link lengths beyond 7.5 m and 3.5 MHz, did not prevent the transmission over links of 5 m, considering a signal frequency of 10 MHz.

Illumination standards for general IC and ward environment lighting were satisfied, as all distances have multiple measurements between 200 and 1000 lux respectively. The satisfactory multiple results demonstrate the susceptibility of the system with correct signal reception at dimmed illumination values below 20 and 5 lux, marking the observation/night light standards in the respective environments. Therefore, it is possible to conclude that the evaluated VLC system can perfectly be applied in such scenario, especially if an LED bias current of 400 mA, an OOK signal frequency of 1 MHz and a link length of 2.5 m are considered.

Moreover, the transmission of data generated by the sensors of the multi-parametric monitor via the designed VLC system with Manchester line codification was successfully demonstrated in this work. The stable and reliable experimental setup, intentionally prepared, confirmed the ability of LEDs to also serve as information access points in areas such as intensive care medical environments. Vital parameters such as heart-rate, oxygen saturation, pulse rate, respiration rate, temperature and non-intrusive blood pressure of a multi-parametric patient monitor were successfully transmitted and recovered with the experimental setup. The captured vital parameters were sent considering an LED polarization current of 400 mA, at VLC distances of 1.5, 5 and 15 m. The results obtained with the multi-parametric monitor provide EOP values of 0.89, 0.96 and 2.67 dB at the equivalent link distances. This final evaluation proved the feasibility of the proposed VLC system as an interesting technology in classified intensive care medical environments, preventing electromagnetic interference on vital equipment, with a low-cost and straightforward solution, respecting human well-being by a flicker-free and on demand illuminance dimmable wireless data transmission over variable distances, along with additional support of prevention spreading emerging diseases.

As future works, it is suggested to improve the detection and recovery of the Manchester symbols to reduce harmonics with relative high amplitudes, as well as interference introduced by different sources in the same frequency range. In terms of signal reception with low light intensities, the adoption of a more diffuse luminaire and the impact of the optical modulation index parameter can be investigated. To understand the limits of the system, a maximum EOP level for signal detection should be defined, depending on up-sampling factors, noise levels, among others. Stand-alone electronic improvement should be considered in a real-time data treatment, utilizing for example, a high speed

microcontroller or an FPGA with transceiver integrated circuits for signal conditioning and simplicity. Reception of patient's vital parameters at a specialist owned smartphone by its camera or sensors can now be exploited to show vital data along with alerts, that can help to shorten the time between intervention in hospitals.

Bibliography

1 CISCO. *Cisco Annual Internet Report*. 2020. <https://www.cisco.com/c/en/us/solutions/executive-perspectives/annual-internet-report/index.html>. [Online; accessed 25-April-2020]. Cited 2 times in pages 15 and 2.

2 HAAS, H. *High-speed wireless networking using visible light*. 2013. <https://spie.org/news/4773-high--speed-wireless-networking-using-visible-light?SSO=1>. [Online; accessed 4-April-2020]. Cited 2 times in pages 15 and 12.

3 BI, W. W. et al. *Handbook of GaN Semiconductor Materials and Devices*. [S.l.]: CRC Press, 2017. Cited 2 times in pages 15 and 14.

4 KARUNATILAKA, D. et al. Led based indoor visible light communications: State of the art. *IEEE communications surveys and tutorials*, v. 17, n. 3, p. 1649–1678, 2015. Cited 2 times in pages 17 and 15.

5 WILLNER, A. *Optical fiber telecommunications*. [S.l.]: Academic Press, 2019. v. 11. Cited 2 times in pages 17 and 15.

6 FOSCO. *Pin fotodetector characteristics for optical fiber communication*. 2016. <https://www.fiberoptics4sale.com/blogs/archive-posts/95046662-pin-photodetector-characteristics-for-optical-fiber-communication>. [Online; accessed 7-April-2020]. Cited 2 times in pages 17 and 16.

7 GUPTA, A.; JHA, R. K. A survey of 5g network: Architecture and emerging technologies. *IEEE access*, IEEE, v. 3, p. 1206–1232, 2015. Cited on page. 1.

8 Yang, P. et al. 6g wireless communications: Vision and potential techniques. *IEEE Network*, v. 33, n. 4, p. 70–75, 2019. Cited on page. 1.

9 Schulz, D. et al. Robust optical wireless link for the backhaul and fronthaul of small radio cells. *Journal of Lightwave Technology*, v. 34, n. 6, p. 1523–1532, 2016. Cited on page. 1.

10 Pathak, P. H. et al. Visible light communication, networking, and sensing: A survey, potential and challenges. *IEEE Communications Surveys Tutorials*, v. 17, n. 4, p. 2047–2077, 2015. Cited on page. 1.

11 Hussain, B. et al. Visible light communication system design and link budget analysis. *Journal of Lightwave Technology*, v. 33, n. 24, p. 5201–5209, 2015. Cited on page. 1.

12 ARNON, S. *Visible light communication*. [S.l.]: Cambridge University Press, 2015. Cited 2 times in pages 1 and 11.

13 RAJAGOPAL, S.; ROBERTS, R. D.; LIM, S.-K. Ieee 802.15. 7 visible light communication: modulation schemes and dimming support. *IEEE Communications Magazine*, IEEE, v. 50, n. 3, 2012. Cited 5 times in pages 1, 3, 13, 21, and 22.

14 BERENGUER, P. W. et al. Optical wireless mimo experiments in an industrial environment. *IEEE Journal on Selected Areas in Communications*, IEEE, v. 36, n. 1, p. 185–193, 2017. Cited on page. 1.

15 MAHMOOD, Z. *The Internet of Things in the Industrial Sector*. [S.l.]: Springer, 2019. Cited on page. 1.

16 RETAMAL, J. R. D. et al. 4-gbit/s visible light communication link based on 16-qam ofdm transmission over remote phosphor-film converted white light by using blue laser diode. *Optics express*, Optical Society of America, v. 23, n. 26, p. 33656–33666, 2015. Cited on page. 1.

17 KHAN, L. U. Visible light communication: Applications, architecture, standardization and research challenges. *Digital Communications and Networks*, Elsevier, v. 3, n. 2, p. 78–88, 2017. Cited 2 times in pages 1 and 3.

18 SERAFIMOVSKI, N. et al. Light communications for wireless local area networking. *IEEE 5G Tech Focus*, v. 2, 2018. Cited on page. 2.

19 RACHIM, V. P. et al. Demonstration of long-distance hazard-free wearable eeg monitoring system using mobile phone visible light communication. *Optics express*, Optical Society of America, v. 25, n. 2, p. 713–719, 2017. Cited on page. 3.

20 RACHIM, V. P. et al. A novel smartphone camera-led communication for clinical signal transmission in mhealth-rehabilitation system. In: IEEE. *2017 39th Annual International Conference of the IEEE Engineering in Medicine and Biology Society (EMBC)*. [S.l.], 2017. p. 3437–3440. Cited on page. 3.

21 WHO. *eHealth*. 2020. <https://www.who.int/ehealth/en/>. [Online; accessed 22-April-2020]. Cited on page. 3.

22 SONG, J. et al. Indoor hospital communication systems: An integrated solution based on power line and visible light communication. In: IEEE. *Faible Tension Faible Consommation (FTFC), 2014 IEEE*. [S.l.], 2014. p. 1–6. Cited on page. 3.

23 AUTHOR. *Demonstration of hospitals equipment transportation and wired connection*. 2020. Movie demonstrated during defence of this Dissertation. Demonstration only intended to motivate this work. Cited on page. 3.

24 Arfaoui, M. A. et al. Physical layer security for visible light communication systems: A survey. *IEEE Communications Surveys Tutorials*, p. 1–1, 2020. Cited on page. 3.

25 ASSOCIATION, I. et al. Ieee standard for local and metropolitan area networks-part 15.7: short-range wireless optical communication using visible light. *IEEE Std*, v. 802, p. 7–2011, 2011. Cited 3 times in pages 3, 21, and 26.

26 DILAURA, D. L. et al. *The lighting handbook: Reference and application*. [S.l.]: Illuminating Engineering Society of North America New York, 2011. Cited 2 times in pages 3 and 21.

27 MEJIA, C. E. et al. Code design for flicker mitigation in visible light communications using finite state machines. *IEEE Transactions on Communications*, IEEE, v. 65, n. 5, p. 2091–2100, 2017. Cited 2 times in pages 3 and 21.

28 SHAILESH, K.; SHAILESH, T. Review of photometric flicker metrics and measurement methods for led lighting. In: IEEE. *Advanced Computing and Communication Systems (ICACCS), 2017 4th International Conference on*. [S.l.], 2017. p. 1–7. Cited 2 times in pages 3 and 21.

29 RAMOS, S. G. et al. Experimental evidences for visual evoked potentials with stimuli beyond the conscious perception threshold. In: IEEE. *Biosignals and Biorobotics Conference (BRC), 2011 ISSNIP*. [S.l.], 2011. p. 1–5. Cited 2 times in pages 4 and 22.

30 ADIONO, T. et al. Visible light communication system for wearable patient monitoring device. In: IEEE. *2016 IEEE Region 10 Conference (TENCON)*. [S.l.], 2016. p. 1969–1972. Cited on page. 4.

31 TORKESTANI, S. S. et al. Indoor optical wireless system dedicated to healthcare application in a hospital. *IET communications*, IET, v. 6, n. 5, p. 541–547, 2012. Cited on page. 4.

32 MANA, S. M. et al. Lifi experiments in a hospital. In: OPTICAL SOCIETY OF AMERICA. *Optical Fiber Communication Conference*. [S.l.], 2020. p. M3I–2. Cited on page. 4.

33 MAYURI, M.; VIJAYALAKSHMI, B.; SINDHUBALA, K. Biomedical data transmission using visible light communication. *International Journal of Applied Engineering Research*, v. 10, n. 20, p. 2015. Cited on page. 4.

34 BADIZADEGAN, N. D. et al. Radiofrequency interference in the clinical laboratory: Case report and review of the literature. *American journal of clinical pathology*, Oxford University Press US, v. 151, n. 5, p. 522–528, 2019. Cited on page. 4.

35 CHEONG, Y.-K.; NG, X.-W.; CHUNG, W.-Y. Hazardless biomedical sensing data transmission using vlc. *IEEE sensors journal*, IEEE, v. 13, n. 9, p. 3347–3348, 2013. Cited on page. 4.

36 TEJA, T. B.; TEJU, V. Experimental biomedical ecg signal transmission using vlc. 2016. Cited on page. 4.

37 DHATCHAYENY, D. R. et al. A novel optical body area network for transmission of multiple patient vital signs. In: IEEE. *2017 Ninth International Conference on Ubiquitous and Future Networks (ICUFN)*. [S.l.], 2017. p. 542–544. Cited on page. 4.

38 DHATCHAYENY, D. R. et al. Eeg biomedical signal transmission using visible light communication. In: IEEE. *2015 International Conference on Industrial Instrumentation and Control (ICIC)*. [S.l.], 2015. p. 243–246. Cited on page. 4.

39 KUMARI, U.; SAMIAPPAN, D. All optical health monitoring system: An experimental study on visible light communication in biomedical signal transmission. In: _____. [S.l.: s.n.], 2018. p. 361–370. ISBN 978-981-10-3811-2. Cited on page. 4.

40 LUCKYARNO, Y. F.; CHERNTANOMWONG, P.; WIJAYA, R. Posturometry data transmission using visible light communication. In: IEEE. *2016 13th International Conference on Electrical Engineering/Electronics, Computer, Telecommunications and Information Technology (ECTI-CON)*. [S.l.], 2016. p. 1–4. Cited on page. 4.

41 CAHYADI, W. A. et al. Patient monitoring using visible light uplink data transmission. In: IEEE. *2015 International Symposium on Intelligent Signal Processing and Communication Systems (ISPACS)*. [S.l.], 2015. p. 431–434. Cited on page. 4.

42 HUANG, C.; ZHANG, X. Impact and feasibility of darklight led on indoor visible light positioning system. In: IEEE. *2017 IEEE 17th International Conference on Ubiquitous Wireless Broadband (ICUWB)*. [S.l.], 2017. p. 1–5. Cited on page. 4.

43 ILAKKIASELVAN, D. et al. Real time biomedical signal transmission using visible light communication. Cited on page. 5.

44 DING, W. et al. A hybrid power line and visible light communication system for indoor hospital applications. *Computers in industry*, Elsevier, v. 68, p. 170–178, 2015. Cited on page. 5.

45 MURAI, R. et al. A novel visible light communication system for enhanced control of autonomous delivery robots in a hospital. In: IEEE. *2012 IEEE/SICE International Symposium on System Integration (SII)*. [S.l.], 2012. p. 510–516. Cited on page. 5.

46 UYSAL, M. et al. *Optical wireless communications: an emerging technology*. [S.l.]: Springer, 2016. Cited on page. 11.

47 BOUCHET, O. et al. *Free-space optics: propagation and communication*. [S.l.]: John Wiley & Sons, 2010. v. 91. Cited on page. 11.

48 DIMITROV, S.; HAAS, H. *Principles of LED light communications: towards networked Li-Fi*. [S.l.]: Cambridge University Press, 2015. Cited on page. 11.

49 GHASSEMLOOY, Z.; POPOOLA, W.; RAJBHANDARI, S. *Optical wireless communications: system and channel modelling with Matlab®*. [S.l.]: CRC press, 2012. Cited 3 times in pages 11, 12, and 17.

50 PATTISON, P. M.; HANSEN, M.; TSAO, J. Y. Led lighting efficacy: status and directions. *Comptes Rendus Physique*, Elsevier, v. 19, n. 3, p. 134–145, 2018. Cited on page. 11.

51 HUANG, Y.-F. et al. 17.6-gbps universal filtered multi-carrier encoding of gan blue ld for visible light communication. In: IEEE. *Lasers and Electro-Optics (CLEO), 2017 Conference on*. [S.l.], 2017. p. 1–2. Cited on page. 11.

52 CHUN, H. et al. A wide-area coverage 35 gb/s visible light communications link for indoor wireless applications. *Scientific reports*, Nature Publishing Group, v. 9, n. 1, p. 1–8, 2019. Cited on page. 11.

53 LETI cea. *CEA-Leti Researchers Breakthrough put Record for LiFi Communications Using Single GaN Blue Micro-Light-Emitting Diode*. 2020. <http://www.cea.fr>. [Online; accessed 23-June-2020]. Cited on page. 11.

54 GHASSEMLOOY, Z. et al. Emerging optical wireless communications-advances and challenges. *IEEE journal on selected areas in communications*, IEEE, v. 33, n. 9, p. 1738–1749, 2015. Cited on page. 11.

55 HAAS, H. Lifi is a paradigm-shifting 5g technology. *Reviews in Physics*, Elsevier, v. 3, p. 26–31, 2018. Cited on page. 12.

56 LEE, C.-C. *The current trends of optics and photonics*. [S.l.]: Springer, 2014. v. 129. Cited on page. 12.

57 ANTTALAINEN, T. *Introduction to telecommunications network engineering*. [S.l.]: Artech House, 2003. Cited on page. 12.

58 AYUB, S. et al. A practical approach of vlc architecture for smart city. In: IEEE. *2013 Loughborough Antennas & Propagation Conference (LAPC)*. [S.l.], 2013. p. 106–111. Cited on page. 13.

59 HAAS, H. et al. What is lifi? *Journal of Lightwave Technology*, IEEE, v. 34, n. 6, p. 1533–1544, 2016. Cited on page. 13.

60 CARMO, R. *Sistemas de comunicações óticas em espaço livre explorando formatos de modulação avançados*. 2017. Cited 2 times in pages 13 and 18.

61 KUMAR, N.; LOURENCO, N. R. Led-based visible light communication system: a brief survey and investigation. *J. Eng. Appl. Sci*, v. 5, n. 4, p. 296–307, 2010. Cited on page. 13.

62 PANG, G. et al. Led traffic light as a communications device. In: IEEE. *Intelligent Transportation Systems, 1999. Proceedings. 1999 IEEE/IEEJ/JSAI International Conference on*. [S.l.], 1999. p. 788–793. Cited on page. 13.

63 KOMINE, T.; NAKAGAWA, M. Integrated system of white led visible-light communication and power-line communication. *IEEE Transactions on Consumer Electronics*, IEEE, v. 49, n. 1, p. 71–79, 2003. Cited on page. 13.

64 LORENTZ, K.; MARUES, J. G.; MONTEIRO, T. *Díodos emissores de luz e iluminação*. 2015. <https://www.spf.pt/magazines/GFIS/119/article/991/pdf>. [Online; accessed 6-April-2020]. Cited on page. 13.

65 CARTLEDGE, J. C. et al. Digital signal processing for fiber nonlinearities. *Optics express*, Optical Society of America, v. 25, n. 3, p. 1916–1936, 2017. Cited on page. 14.

66 COSSU, G. et al. 3.4 gbit/s visible optical wireless transmission based on rgb led. *Optics express*, Optical Society of America, v. 20, n. 26, p. B501–B506, 2012. Cited on page. 14.

67 LI, H. et al. A 550 mbit/s real-time visible light communication system based on phosphorescent white light led for practical high-speed low-complexity application. *Optics express*, Optical Society of America, v. 22, n. 22, p. 27203–27213, 2014. Cited 3 times in pages 14, 64, and 65.

68 DUTTON, H. J. *Understanding optical communications*. [S.l.]: Prentice Hall PTR New Jersey, 1998. Cited on page. 14.

69 GHASSEMLOOY, Z. et al. *Visible Light Communications: Theory and Applications*. [S.l.]: CRC Press, 2017. Cited 2 times in pages 15 and 27.

70 PAL, B. P. *Fundamentals of fibre optics in telecommunication and sensor systems*. [S.l.]: Bohem press, 1992. Cited on page. 15.

71 QIU, Y.; CHEN, H.-H.; MENG, W.-X. Channel modeling for visible light communications—a survey. *Wireless Communications and Mobile Computing*, Wiley Online Library, v. 16, n. 14, 2016. Cited on page. 16.

72 KAHN, J. M.; BARRY, J. R. Wireless infrared communications. *Proceedings of the IEEE*, IEEE, v. 85, n. 2, p. 265–298, 1997. Cited on page. 17.

73 QUAN, J.; LI, Y.; ZHANG, Y. Configuring indoor visible light communication networks. In: IEEE. *Communications in China Workshops (ICCC), 2012 1st IEEE International Conference on*. [S.l.], 2012. p. 54–58. Cited on page. 17.

74 KOMINE, T.; NAKAGAWA, M. Fundamental analysis for visible-light communication system using led lights. *IEEE transactions on Consumer Electronics*, IEEE, v. 50, n. 1, p. 100–107, 2004. Cited 2 times in pages 17 and 18.

75 NASER, S. et al. Rate-splitting multiple access: Unifying noma and sdma in miso vlc channels. *arXiv preprint arXiv:2007.13560*, 2020. Cited on page. 18.

76 ELGALA, H.; MESLEH, R.; HAAS, H. An led model for intensity-modulated optical communication systems. *IEEE Photonics Technology Letters*, IEEE, v. 22, n. 11, p. 835–837, 2010. Cited on page. 19.

77 LEHMAN, B. et al. Proposing measures of flicker in the low frequencies for lighting applications. In: IEEE. *Energy Conversion Congress and Exposition (ECCE), 2011 IEEE*. [S.l.], 2011. p. 2865–2872. Cited on page. 21.

78 HONG, Y.; XU, J.; CHEN, L.-K. Experimental investigation of multi-band oct precoding for ofdm-based visible light communications. *Optics express*, Optical Society of America, v. 25, n. 11, p. 12908–12914, 2017. Cited on page. 22.

79 YESILKAYA, A. et al. Optical mimo-ofdm with generalized led index modulation. *IEEE Transactions on Communications*, IEEE, v. 65, n. 8, p. 3429–3441, 2017. Cited on page. 22.

80 HONG, Y.; CHEN, L.-K.; GUAN, X. Adaptive physical-layer network coding over visible light communications. In: OPTICAL SOCIETY OF AMERICA. *Optical Fiber Communication Conference*. [S.l.], 2017. p. Th1E–4. Cited on page. 22.

81 LIU, S.-a. et al. Experimental research of adaptive ofdm and oct precoding with a high se for vllc system. *Optical Fiber Technology*, Elsevier, v. 37, p. 21–25, 2017. Cited on page. 22.

82 DALARMELINA, C. A. et al. Evaluation of selective control information detection scheme in orthogonal frequency division multiplexing-based radio-over-fiber and visible light communication links. *Optical Engineering*, International Society for Optics and Photonics, v. 56, n. 5, p. 056108, 2017. Cited on page. 22.

83 NEE, R. v.; PRASAD, R. *OFDM for wireless multimedia communications*. [S.l.]: Artech House, Inc., 2000. Cited on page. 22.

84 BARROS, D. J.; KAHN, J. M. Optimized dispersion compensation using orthogonal frequency-division multiplexing. *Journal of Lightwave Technology*, IEEE, v. 26, n. 16, p. 2889–2898, 2008. Cited on page. 22.

85 BANDARA, K.; NIROOPAN, P.; CHUNG, Y.-H. Papr reduced ofdm visible light communication using exponential nonlinear companding. In: IEEE. *Microwaves, Communications, Antennas and Electronics Systems (COMCAS), 2013 IEEE International Conference on*. [S.l.], 2013. p. 1–5. Cited on page. 23.

86 YU, Z.; BAXLEY, R. J.; ZHOU, G. T. Iterative clipping for papr reduction in visible light ofdm communications. In: *Military Communications Conference*. [S.l.: s.n.], 2014. p. 1681–1686. Cited on page. 23.

87 OGUNKOYA, F. et al. Performance evaluation of pilot-assisted papr reduction technique in optical ofdm systems. *IEEE Photonics Technology Letters*, IEEE, v. 27, n. 10, p. 1088–1091, 2015. Cited on page. 23.

88 HU, W.-W.; LEE, D.-H. Papr reduction for visible light communication systems without side information. *IEEE Photonics Journal*, IEEE, v. 9, n. 3, p. 1–11, 2017. Cited on page. 23.

89 SILVA, J. A.; CARTAXO, A. V.; SEGATTO, M. E. A papr reduction technique based on a constant envelope ofdm approach for fiber nonlinearity mitigation in optical direct-detection systems. *Journal of Optical Communications and Networking*, Optical Society of America, v. 4, n. 4, p. 296–303, 2012. Cited 2 times in pages 23 and 25.

90 NUNES, R. B. et al. Experimental validation of a constant-envelope ofdm system for optical direct-detection. *Optical Fiber Technology*, Elsevier, v. 20, n. 3, p. 303–307, 2014. Cited 3 times in pages 23, 25, and 42.

91 SINGH, V. K.; DALAL, U. Abatement of papr for aco-ofdm deployed in vlc systems by frequency modulation of the baseband signal forming a constant envelope. *Optics Communications*, Elsevier, v. 393, p. 258–266, 2017. Cited on page. 23.

92 LI, Y.; DING, D. Investigation into constant envelope orthogonal frequency division multiplexing for polarization-division multiplexing coherent optical communication. *Optical Engineering*, International Society for Optics and Photonics, v. 56, n. 9, p. 096108, 2017. Cited on page. 23.

93 PEREIRA, E. d. V. et al. Impact of optical power in the guard-band reduction of an optimized ddo-ofdm system. *Journal of Lightwave Technology*, IEEE, v. 33, n. 23, p. 4717–4725, 2015. Cited on page. 24.

94 WANG, Z. et al. *Visible Light Communications: Modulation and Signal Processing*. [S.l.]: John Wiley & Sons, 2017. Cited on page. 26.

95 PROAKIS, J.; SALEHI, M. *Digital communications*. [S.l.]: McGraw-hill New York, 2001. v. 4. Cited on page. 26.

96 IEEE Standard for Ethernet. *IEEE Std 802.3-2018 (Revision of IEEE Std 802.3-2015)*, p. 1–5600, 2018. Cited on page. 26.

97 BINH, L. *Optical fiber communication systems with Matlab and Simulink models in*. [S.l.]: CRC Press, 2014. Cited 2 times in pages 28 and 29.

98 STEPHENS, R. Jitter analysis: The dual-dirac model, rj/dj, and q-scale. *Agilent Technical Note*, 2004. Cited on page. 29.

99 LUMILEDS. *LUXEON Rebel ES - Datasheet*. 2020. <https://www.lumileds.com/uploads/17/DS61-pdf>. [Online; accessed 4-April-2020]. Cited 2 times in pages 32 and 33.

100 SILVA, F. B. da; MARTINS, W. A. A computational platform for visible light communications. *XXXV Simpósio Brasileiro de Telecomunicações e Processamento de Sinais (SBrT 2017)*, p. 891–895, 2017. Cited on page. 37.

101 ZWAAG, K. et al. Adaptation to the leds flicker requirement in visible light communication systems through ce-ofdm signals in. *Optics Communications*, v. 441, p. 14 – 20, 2019. Cited 2 times in pages 42 and 64.

102 ZWAAG, K. vd et al. Increasing vlc nonlinearity tolerance by ce-ofdm. In: OPTICAL SOCIETY OF AMERICA. *Latin America Optics and Photonics Conference*. [S.l.], 2018. p. W3D–3. Cited on page. 43.

103 2011, B. S. I. B. E. .-. *Light and Lighting–Lighting of Work Places–Part 1: Indoor Work Places*. [S.l.]: BSI London, 2011. Cited on page. 47.

104 INTERNATIONAL, H. *Health Level 7 standard*. 2020. <https://www.hl7.org/index.cfm>. [Online; accessed 8-April-2020]. Cited on page. 48.

105 INOUE, K. Waveform distortion in a gain-saturated semiconductor optical amplifier for nrz and manchester formats. *IEE Proceedings-Optoelectronics*, IET, v. 144, n. 6, p. 433–437, 1997. Cited on page. 63.

106 LEE, S.-H. Flicker-free visible light communication using three-level rz modulation. *Journal of Sensor Science and Technology*, The Korean Sensors Society, v. 29, n. 2, p. 75–81, 2020. Cited on page. 64.

107 LI, H. et al. High-speed phosphorescent white led visible light communications without utilizing a blue filter. *Chinese Optics Letters*, Chinese Optical Society, v. 13, n. 8, p. 080605, 2015. Cited on page. 65.

108 BIAN, R.; TAVAKKOLNIA, I.; HAAS, H. 15.73 gb/s visible light communication with off-the-shelf leds. *Journal of Lightwave Technology*, IEEE, v. 37, n. 10, p. 2418–2424, 2019. Cited on page. 65.

APPENDIX A – Performance Comparison among Manchester Eye Patterns

The obtained results exposed performance differences among both Manchester half symbol periods (eyes). It was noticed that the first eye, compared to the second, exhibits a reduced performance at lower frequencies. However, contrarily better performance at higher frequencies occurred, as in [105] where is shown that Manchester symbol can be sampled in the first or the second half. Figure 40 shows both eyes with the eye opening penalty as function of the bias current and frequency.

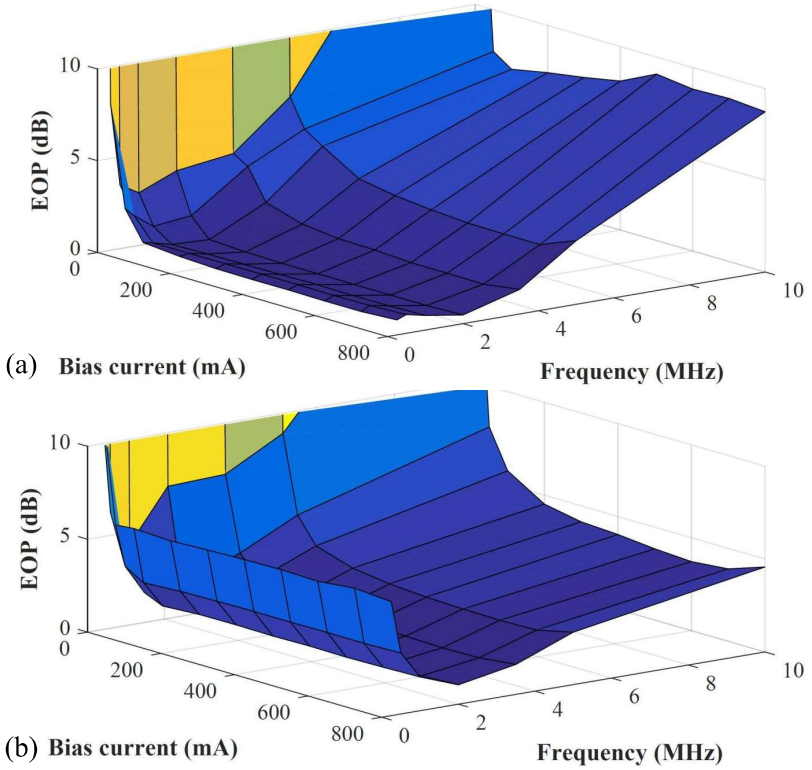

Figure 40 – Detail of the measured EOP of the first eye (a) and second (b) as function of current at a distance of 3 m.

Some preliminary experiments demonstrated stable signal reception when recovery was based on the second eye with frequencies from 250 kHz up to 10 MHz. The first one showed a surprisingly better performance with frequencies of up to 30 MHz. It should be noted that the experiments were executed without error handling and as well as the first eye suffers a higher overall penalty at lower frequencies. The aforementioned results can be explained by displaying Manchester's signal patterns in an eye-diagram. The first eye tent to constrict at lower frequencies as can be seen in Figure 34 at 500 kHz, while Figure 41

shows an improved eye due to its nonlinearities at higher frequencies.

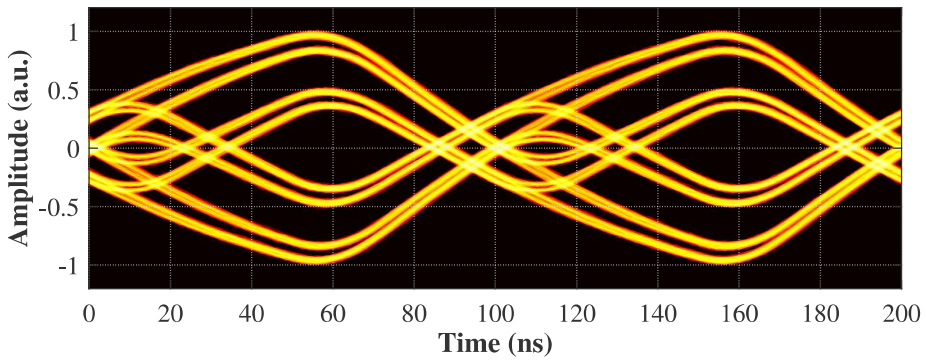

Figure 41 – Eye-diagram at 10 MHz at 400 mA LED polarization current and 3 m transmission link.

An algorithm could be used to select what eye pattern should be utilized for decoding. To detect lower frequencies, frequencies below <100 kHz, impulse registration can be applied like in [106]. On the other hand, simple and low cost pre-emphasis and/or pos-equalization techniques, eliminating LEDs limitations, can be applied to increase the bandwidth as demonstrated in [101, 67].

APPENDIX B – Receiver Prototype Schematics

For this work, two distinct receivers were developed and employed in the experiments. At first, a receiver was designed based on the works described in [67, 107]. This receiver operated properly for sinusoidal signals, however an internal DC-cancellation in the transimpedance amplifier MAX3665, blocked square-wave signals below 5 MHz. Due to the nature of this research, the second prototype was based on [108] and designed to receive signals of 25 kHz till 250 MHz.

A difference is that the former prototype is equipped with more advanced differential components and filters while the latter consists of off-the-shelf components. Despite these differences a performance comparison with a 5 MHz 16-QAM OFDM signal, similar results were shown, while component costs dropped from 124 to 15 $, respectively. Both prototype schematics are shown on the subsequent pages.

VLC Receiver with Amplification and Post-Emphasis

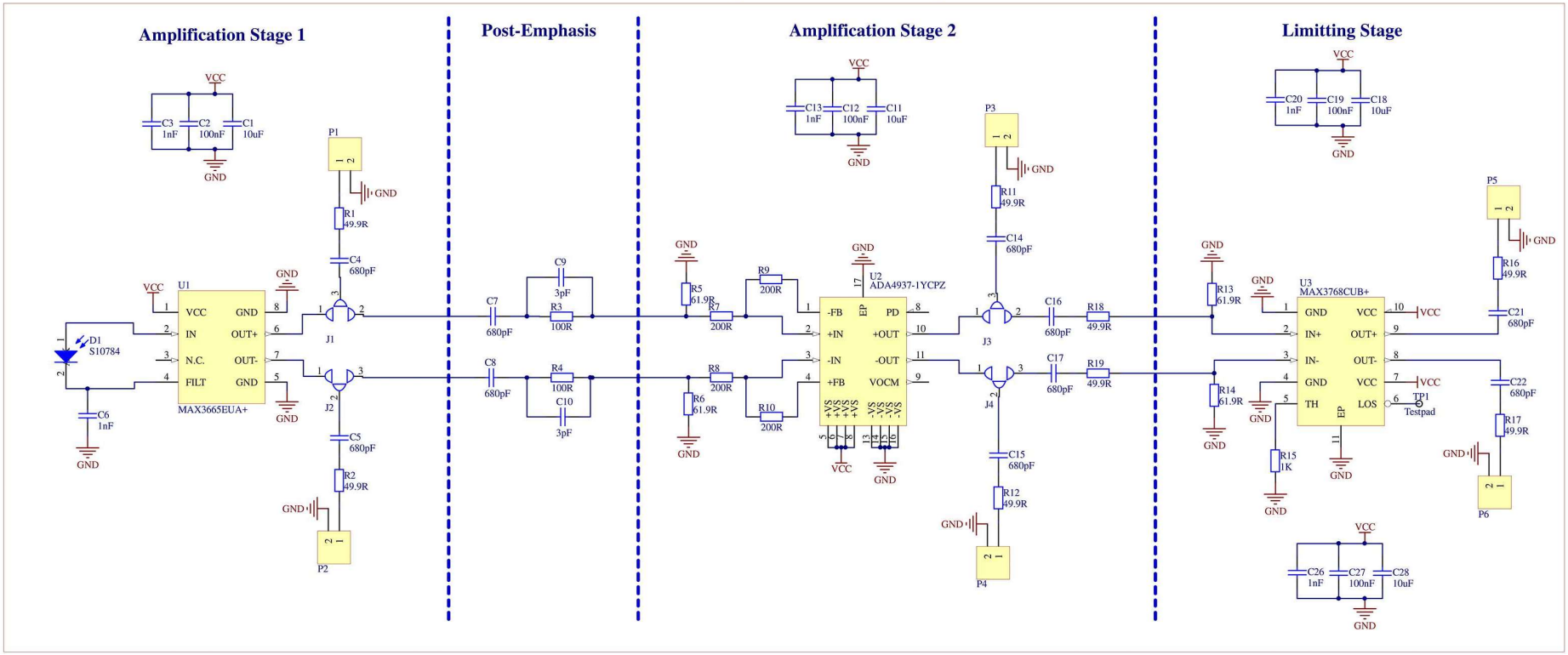

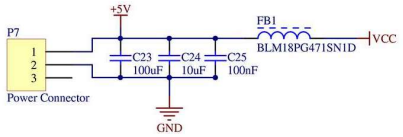

Title	*VLC Receiver 2Solve/Labtel*		
Size: A3	Number:*	Revision:1	
Date: 06-Aug-18	Time: 3:48:44 PM	Sheet 1 of 1	
File: VLC Schematic UFES.SchDoc			Author: Klaas van der Zwaag

Amplification Stage

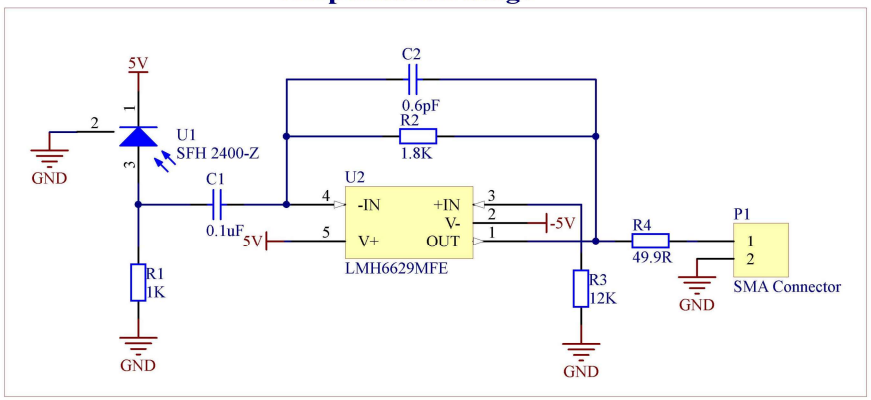

Power

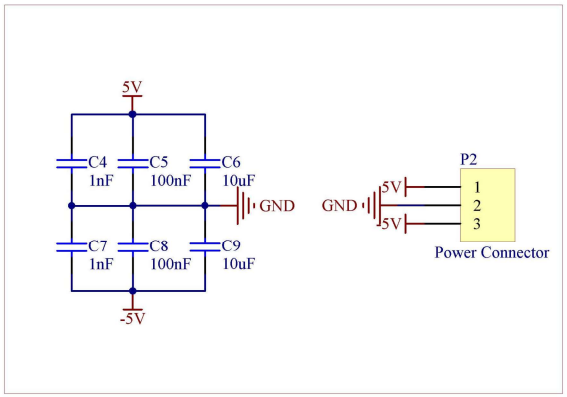

Title	*VLC Receiver 2solve/Labtel V2*		
Size: A4	Number: 1	Revision:	
Date: 1-7-2020	Time: 00:16:01	Sheet 1 of 1	
File: VLC Receptor UFES V2.SchDoc		Author: Klaas van der Zwaag	